INVESTIGATING THE CRASHWORTHINESS CHARACTERISTICS OF CARBON FIBER/EPOXY TUBES

by

Marc A. Courteau

A thesis submitted to the faculty of
The University of Utah
in partial fulfillment of the requirements for the degree of

Master of Science

Department of Mechanical Engineering

The University of Utah

December 2011

The University of Utah Graduate School

STATEMENT OF THESIS APPROVAL

The thesis of **Marc A. Courteau**

has been approved by the following supervisory committee members:

Dan Adams	, Chair	**7/8/2011** Date Approved
K. Larry DeVries	, Member	**7/8/2011** Date Approved
Brittany Coats	, Member	**7/8/2011** Date Approved

and by **Timothy Ameel**, Chair of the Department of **Mechanical Engineering**

and by Charles A. Wight, Dean of The Graduate School.

ABSTRACT

As composite materials are integrated into the primary structures of today's vehicles, it is important that their crashworthiness characteristics are well understood. This research focuses on the energy absorption mechanisms that occur in composite tubes during axial crushing and how those mechanisms are affected by material, geometric, and testing variables.

A literature review was completed on composite tube testing for crashworthiness applications to provide background information on the subject. Methods of measuring crashworthiness performance were introduced as well as the three broad classifications of failure modes that occur during axial crushing. Fiber and matrix type, preform type, specimen geometry, trigger type, and strain rate were all found to have a significant effect on the amount of energy composite tubes absorbed. It was observed that several of these variable effects on carbon fiber prepreg/epoxy tubes were not well agreed upon, allowing for additional investigation.

Based on observations from the literature an investigation into strain rate and triggering effects was performed on IM7/8552 prepreg tubes. Three layups were designed to represent the three broad classifications of failure modes. Circular and square cross tubes were used to test the effect of bevel and tulip triggers at both quasi-static and dynamic test speeds for all failure modes. Circular cross sections were found to be more

efficient that square cross sections when comparing similar test variables. Tulip triggers were found to increase energy absorption for the brittle fracture and fiber splaying failure modes at quasi-static test speeds. Strain rate effects varied widely across layups, trigger types, and cross sectional shapes and were attributed to changes in failure mode. It was found that the brittle behavior of the 8552 matrix at high strain rates was responsible for this behavior.

TABLE OF CONTENTS

ACKNOWLEDGEMENTS

I would like to thank all of the individuals who have made contributions to this thesis. I would like to thank Dr. Dan Adams, my advisor, for his continual guidance and assistance with this project. His knowledge, experience, and good sense of humor kept me on track and pushing forward through any difficulties I encountered. I would also like to thank my other committee members, Dr. Larry DeVries and Dr. Brittany Coats, for their advice and contributions.

I would like to thank the Automotive Composites Consortium (ACC) for their direction and financial support of this project. I would also like to thank the members of the Structural Integrity Lab (SIL) at the University of Utah for their involvement, including many hours preparing test samples.

In addition, I would like to thank my family and all those who have impacted my life in a positive way. I would like to thank my girlfriend, Sarah, who is a continuously wonderful and understanding partner. Finally, I am forever thankful to my parents, Roger and Mary, who taught me the value of hard work and supported whatever goals I strived for. This would not have been possible without you.

1 INTRODUCTION

Composite materials are currently popular in performance-based vehicles due to their high specific strength and stiffness. However, as composite materials become cheaper and more widely available there is a desire to incorporate them into passenger vehicles to reduce weight, part count, and cost. Lighter vehicles would translate to better fuel economy, which is increasingly important in today's world.

Equally important is the safety of occupants during the event of a crash. The ability of a vehicle to survive a collision and protect its passengers from the harmful forces that result is known as crashworthiness. This vehicle trait relies on the vehicle structure absorbing energy during a collision through controlled failure mechanisms. It is important that crashworthiness performance is equaled or improved as composite materials replace metallic materials in vehicle structures. Composite structures have been shown to have greater specific energy absorption capability than metals, indicating the potential for improved crashworthiness.

Composite material crashworthiness research has been conducted since the end of the 1970s. Initial investigations included mechanical testing and comparison of metal and composite specimens. It was found that unlike metals, energy absorption in composite structures was a function of many variables including fiber and matrix types, cross sectional shapes, stacking sequence, fiber architecture, thickness to diameter ratio, testing rate, and trigger geometry. Due to this fact, numerical methods for predicting energy

absorption in large composite structures are difficult and only now are becoming reliable. The material models for these numerical methods still rely on testing results, and so mechanical testing will continue to remain essential to the field of crashworthiness.

The material presented herein will focus on the mechanical testing of composite tubes. The research is broken into sections with additional documentation contained in Appendices A and B. Section 2 is a literature review on the topic of composite tube testing for crashworthiness applications. It gives an account of previous work on the subject and is the main building block from which the research of this thesis was founded. Section 3 presents research investigating strain rate and triggering effects in carbon fiber/epoxy composite tubes. It expands on several testing variables discussed in Section 2 and attempts to clarify phenomena that are not agreed upon in the literature. Appendix A contains the data analysis procedures used for the research in Section 3. Appendix B contains sample load versus displacement curves from the testing preformed for Section 3.

2 LITERATURE REVIEW

2.1 Abstract

The crashworthiness performance of a composite structure depends largely on its ability to absorb energy through controlled failure mechanisms during crushing. Crush testing of simple specimen geometries, including tubes, is often used to characterize these failure mechanisms. Research has shown that the energy absorption of composite tubes is a function of many variables including material type, fiber architecture, tube geometry, and loading rate. This review focuses on topics associated with composite tube testing for crashworthiness applications including measures of energy absorption, failure modes observed, and a discussion of variables affecting energy absorption during crush testing.

2.2 Introduction

Increased vehicle crashworthiness provides occupants with a greater extent of protection and chance of survival in the event of a severe crash. In the United States crashworthiness standards for automobiles are included in the Federal Motor Vehicle Safety Standards and Regulations 200 series guidelines.[1] Other industries have similarly created crashworthiness requirements, such as rotary-wing aircraft (MIL-STD-1290)[2] and passenger rail (Railway Group GM/RT 2100).[3] All of these standards state that in the event of a crash of specific severity, occupants should not experience forces that are known to cause severe internal injury.

Crashworthiness performance is based largely on absorbing energy through structural deformation or controlled failure. As early as the 1970s it was found that composite structures were capable of high energy-absorption-per-unit-mass values.[4] When compared to metallic materials, composites also have relatively high specific stiffness and strength. Vehicle manufacturers understood the potential for composites to reduce the structural weight of designs while, at the same time, increasing their crashworthiness.

Due to the complex failure mechanisms that occur in composite materials during crush, the use of mechanical testing remains a popular method of determining energy absorbing characteristics. Composite crush testing can be divided into three categories: coupon, element, and structure testing. Coupons are small, inexpensive, and easily fabricated shapes that reveal energy absorption properties related to the composite's constituents. Elements are larger self-supporting specimens including tubes, angles, and channels that incorporate realistic geometries used in many vehicle structures. Structures are full-sized assemblies of elements that make up the entire energy absorbing system of a vehicle. This review paper focuses on investigating the crashworthiness of composite materials through the use of element testing, specifically tubes.

The use of tubular specimens in composite crashworthiness investigations has been actively pursued for more than three decades, and a large amount of literature exists. This review focuses on three primary topics associated with composite element testing for crashworthiness assessments. First, measures of energy absorption during crush testing are reviewed. Second, failure modes observed during composite tube testing are

presented. Finally, variables affecting energy absorption during crush testing are discussed.

2.3 Measurement of Energy Absorption in Composite Crush Testing

In theory, an ideal energy absorbing material exhibits a constant compressive load versus crush displacement response over the entire crush distance. In early studies it was noticed that under the right circumstances composite specimens exhibited this type of behavior.[5] Such behavior, referred to as "progressive failure" or "stable crush," is in contrast to specimens that exhibit a peak load followed by catastrophic failure with minimal follow-on compressive loading.

An axial cross section of a typical tubular specimen is shown in Figure 2.1a). The specimen consists of a circular tube of length L with outer and inner diameters D_1 and D_2, respectively. A common type of trigger mechanism that promotes stable crushing (discussed later) is represented on the top of the specimen as a 45° bevel. The tube is assumed to be crushed between two flat plates at a specified displacement rate. If the composite tube experiences stable crush behavior, it will have post-crush characteristics consistent with Figure 2.1b). The symbol δ represents the displacement of the upper platen and d represents the length of the crush zone, which is the portion of the tube that has sustained damage. Beyond the crush zone, d, the specimen is still in its original state. A debris pile consisting of fragmented fibers and matrix or bent lamina pieces is represented inside the tube volume.

Figure 2.2 shows a typical load versus displacement response for a tube that has experienced stable crushing. The curve begins with an initial linear loading region up to a

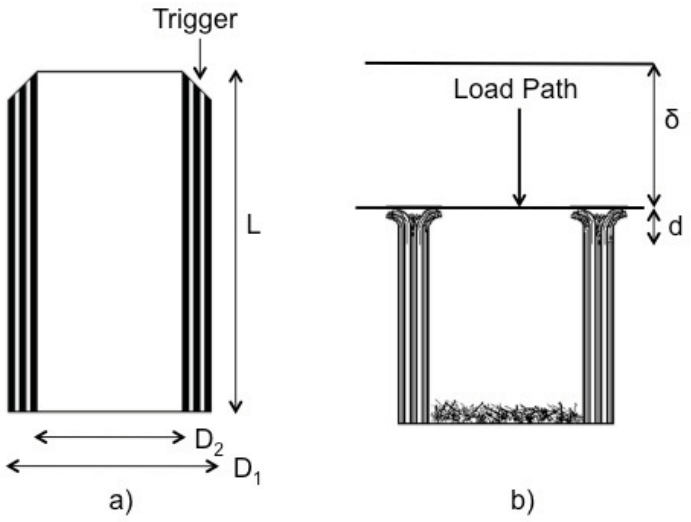

Figure 2.1: Tubular crush specimen: (a) before testing, and (b) after testing.

peak load of p_{max}, resulting from local tube failure at the trigger. This point is labeled δ_1. Following this peak load is the stable crushing region characterized by load serrations at an approximately constant average load, p_{mean}. Finally, when the tube has crushed to an extent where debris on the inside of the tube begins to add to the stiffness of the specimen, the load increases. This displacement corresponds to δ_2.

The area under the load versus displacement curve represents the total energy absorbed by the specimen as it undergoes crushing. The total energy absorbed may be expressed as

$$W = \int_0^{\delta} p dx \tag{2.1}$$

In order to compare data from tubes of various sizes, shapes, or layups as well as from tests performed to different crush distances, the energy absorbed can be normalized as a specific property (per unit mass).

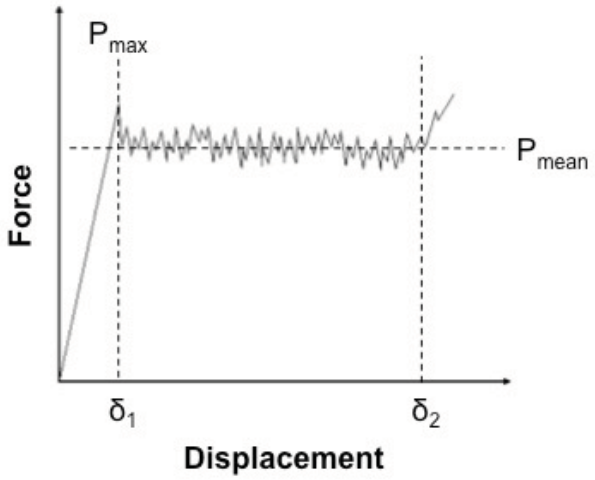

Figure 2.2: Load versus displacement curve for a progressively crushed tube.

There are two commonly used methods of measuring the total energy absorbed per unit mass. The first is by dividing W by the product of area, density, and the crushed length of the tube. This value is known as the specific energy absorption (SEA), E_s. For composite tube specimens utilizing carbon and glass fiber the crush zone, d, has been reported to be relatively small (on the order of the wall thickness of the tube). Further, the crush zone does not change in length significantly with cross head displacement.[6,7] For this reason, the crushed length of the tube used in the calculation of SEA can simply be the displacement of the platen, δ.[8-11] Assuming constant section properties and density, E_s may be expressed as

$$E_s = \frac{W}{A\rho\delta} \tag{2.2}$$

and is commonly presented in units of kJ/kg or ft·lbf/slug. It should be noted that δ should be large enough such that the crush zone length d is negligible, but never greater

than δ_2. For some applications the energy absorbed per unit volume or unit length may also be presented.

The second common method of measuring energy absorbed per mass is by dividing the average crush stress, $\overline{\sigma}$, by the density of the material being tested, or

$$\overline{\sigma}_s = \frac{\overline{\sigma}}{\rho} \quad . \tag{2.3}$$

$\overline{\sigma}_s$ is referred to as specific sustained crushing stress (SSCS).[12] The average crush stress $\overline{\sigma}$ is obtained by dividing p_{mean} by the cross sectional area of the tube, A. This measure of energy absorption per mass is considered acceptable because the initial loading portion of the load versus displacement curve is relatively small and the crush length is consistent with the displacement of the load platen. It is assumed that relatively small fluctuations in the force exist in the stable crush region.[6]

The difference between SEA and SSCS is usually small since the key difference is the exclusion of the area under the initial portion of the load versus displacement curve. For this reason, specific energy absorption (SEA) will be used in this review when discussing results from authors that use either of the two measures of energy absorption per unit mass.

For metal and composite tube specimens failing in a folding mode (Figure 2.3), the length of the tube that has undergone crushing (d+δ) at a point in time is typically 1.4 – 1.5 times the displacement of the load platen (δ).[7]

To account for this the total volume of deformed material in the specimen must be considered. Equation (2.2) becomes

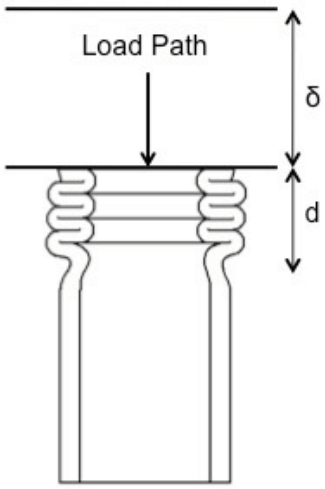

Figure 2.3: Folding failure mode.

$$E_s = \frac{W}{A\rho(\delta + d)} \quad . \tag{2.4}$$

Other measured quantities are often cited when performing crush testing on composite tubes. Stroke efficiency is the measure of the length of stable crushing to the total length of the specimen, or

$$J = \frac{(\delta_2 - \delta_1)}{L} \quad . \tag{2.5}$$

Combing equations (2.2) and (2.5), and assuming that the crosshead displacement is equal to δ_2, gives

$$E_s = \frac{W(\delta_2 - \delta_1)}{m\delta_2} \quad . \tag{2.6}$$

Note that m is the mass of the entire tube specimen. Equation (2.6) takes into account the total distance for which a tube is capable of absorbing energy before debris buildup occurs. For this reason equation (2.6) has been proposed for use in design purposes.[6]

Conversely, equation (2.3) is useful because it does not require integrating the load versus displacement response or require the stroke efficiency. It is therefore representative of the material's capability. However, results still need to be used with caution, as different trigger types have been shown to influence entire load versus displacement response, especially for square and rectangular tubes.[13,14] Due to the potential differences in values obtained using the different measures, it is necessary to include the method of measurement with crush test results.

To evaluate trigger performance a trigger effectiveness, ε_t, has been defined[15] as the ratio of the average crush load, p_{mean}, to the peak load, p_{max}, or

$$\varepsilon_t = \frac{p_{mean}}{p_{\max}} \ . \tag{2.7}$$

A trigger effectiveness of 1.0 would indicate a perfect square wave load versus displacement curve. It has been proposed that values of 0.75 and greater represent well-triggered specimens.[15]

Finally, a quantity known as the Crush Compression Ratio (CCR) is defined as the ratio of the average crush stress to the ultimate compressive strength of the material,[16] or

$$CCR = \frac{\overline{\sigma}}{\sigma_{u,c}} \ . \tag{2.8}$$

A CCR of 0.5 indicates the average crush stress is half of the material compressive strength. This quantity is important during material selection for determining whether a composite structure may fail in compression within the back-up structure due to variations in load as crushing is occurring.

2.4 Failure Modes of Composite Crush Specimens

The crush behavior of composite specimens can be generally classified as either stable or unstable. Unstable crushing is characterized by an initial load peak followed by a sudden catastrophic failure. After this failure the specimen is no longer capable of sustaining a significant compression load. In contrast, stable crushing is characterized by an increase in load until an initial failure occurs. At this point, the specimen, although locally damaged, can still support significant compression loads through further displacement. Although stable crushing results in greater energy absorption and is thus the goal of crashworthy structures, it is important to understand the failure modes associated with both stable and unstable crush behavior.

The relative dimensions of a composite tube specimen play an important role in stable versus unstable failure. The length to diameter (*L/d*) or length to side (*L/s*) ratios are used to express the slenderness of a tube specimen and may be used to predict if buckling will occur. Similarly, the ratio of specimen diameter to wall thickness (*D/t*, circular cross section) or length of a side to wall thickness (*S/t*, square or equilateral triangle cross section) are commonly used. A related property, the relative density ϕ is defined as the ratio of the weight of a tube specimen (either as a whole or per unit length) to that of a solid specimen of the same material and the same external dimensions. The relative density may be expressed as the ratio of cross sectional areas of the tube specimen and a solid specimen, or $A_{specimen}/A_{solid}$. This ratio is useful for reporting non-symmetric or uncommon cross sections.

2.4.1 Unstable Failure Modes

A slender tube may buckle due to column instability (Figure 2.4a). Similarly, interpenetration may occur when the buckling stresses are high enough such that circumferential cracks form near the center of the specimen and the walls split (Figure 2.4b).[7,8] When interpenetration occurs, however, the specimen does not fail entirely and the two halves continue to cleave through one another. Finally, delamination of laminas can occur unstably. Specifically, the outermost 0° layers of a laminate (note: 0° fiber direction is considered to be parallel to the axis of the tube) may bow outward from the inner and outer tube diameter leaving inner layers of the laminate unsupported to fail at lower loads.[6,7,17] This process is known as barreling (Figure 2.4c).

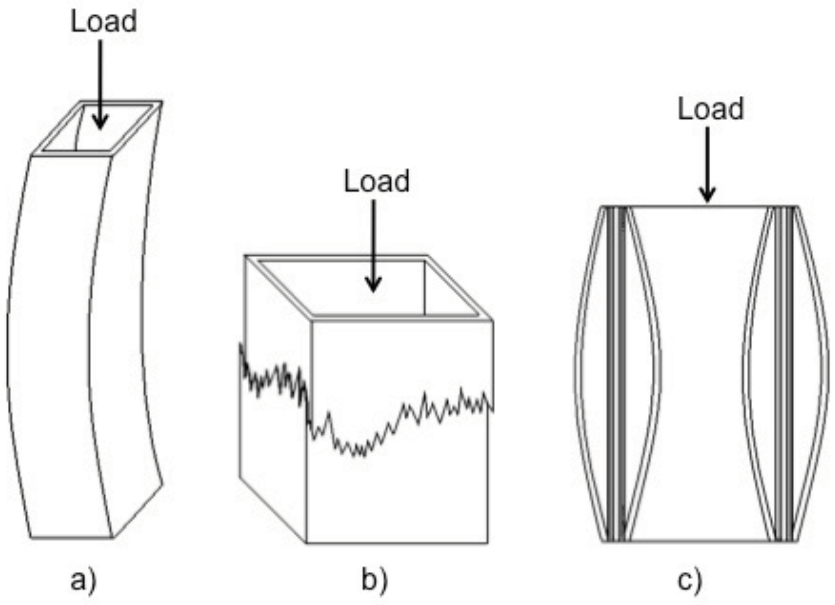

Figure 2.4: Unstable modes of failure showing, (a) buckling, (b) interpenetration, and (c) barreling.

2.4.2 Stable Failure Modes

Numerous failure modes have been observed to take place in a composite structure during stable crushing. The classification and number of these modes varies in the literature. It should be noted that these failure modes might not accurately describe all failures observed in composite tube crush specimens. Hull[7] in 1982 was one of the first to classify and list failure modes associated with stable collapse for E-glass and carbon fiber reinforced composite specimens. Failure modes were classified as fiber splaying and bending, fiber splaying and axial tearing, and micro-fragmentation. In 1985 Kindervater[18] listed failure modes observed on a global scale for glass, carbon, and Kevlar reinforced composites as either fracture or folding.[18] In 1987, Farley[19] classified four crushing modes as local buckling, transverse shearing, brittle fracture, and lamina bending. In 1991 after examination of a wide range of glass and carbon reinforced composite specimens, Hull[6] came to the conclusion that there were two broad types of failure modes: splaying and fragmentation. Jones and Farley in 1992[20] essentially agreed on these failure modes, but named them differently as transverse shearing and lamina bending. A third failure mode was listed as local buckling, which applied to Kevlar and other select fiber reinforced composites. There have been several other proposed classifications of failure modes, and nearly all authors agree that combinations of failure modes are routine due to the number of variables that affect the crush characteristics of composite tube specimens.[6,8,14,18,20]

Failure classifications listed by Hull and Farley are often cited[21,22] after the mid 1990s and are believed to be the current standard for describing stable crushing of composites. The three broad classes of failure modes can be labeled as follows:

Fiber splaying/lamina bending

Fragmentation/transverse shearing

Folding/local buckling/accordion/concertina

The first expression listed above for each classification will be used when referencing failure modes for the remainder of this review. Additionally, the combination of fiber splaying and fragmentation occurs often and is referred to as "brittle fracture." Thus, a total of four stable failure modes have been identified. The key characteristics, failure types produced, and principal energy absorption mechanisms associated with each failure mode are discussed in the Sections 2.4.2.1 – 2.4.2.4.

2.4.2.1 Fiber Splaying

Figure 2.5a) shows a typical cross section of a tube wall that has failed by fiber splaying. The key characteristic of this failure mode is long (greater than laminate thickness) interlaminar, intralaminar, and axial cracks that separate the fibers into bundles, referred to as fronds.[20] These fronds are divided and bent either to the inside or outside of the tube wall and forced through a radius of curvature by the load platen. This radius is dependent upon fiber, matrix, and laminate properties.

As evidenced by the differences of curvature in the fronds and the delamination of the tube wall, shear and tensile stresses develop in the composite during crushing. When these stresses reach critical levels, cracks progress consistent with Mode I and Mode II fracture. Axial cracks have been shown to progress at nearly the same rate as the load platen.[21]

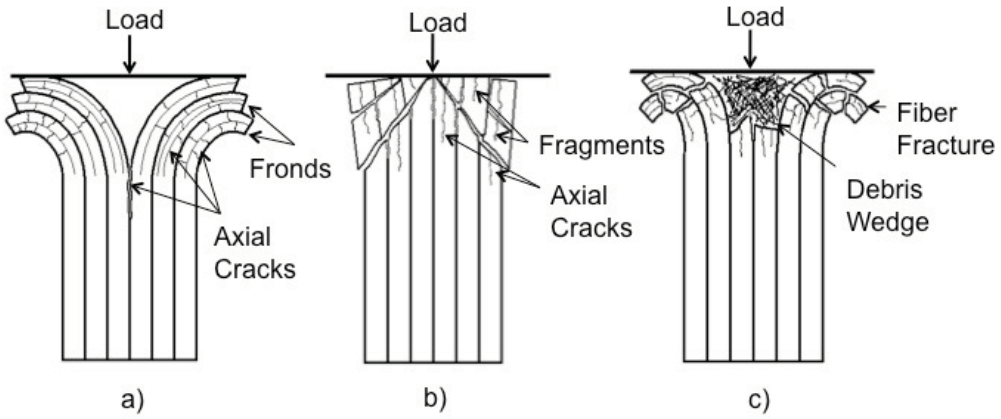

Figure 2.5: Crush failure modes, (a) fiber splaying, (b) fragmentation, and (c) brittle fracture.

Some frond and fiber fracture is expected due to the small radii of curvature away from the load platen.[6,20,21,22] However, if extensive fracture occurs the crush morphology may be better described by the brittle fracture failure mode.

Another possible characteristic of the crush zone for the fiber splaying failure mode is the pile of crushed resin and fibers that accumulates in the gap between external and internal bending fronds. Known as the debris wedge, it generally forms during the initial crush stage as stable mechanisms are developing. This debris wedge becomes more important as it increases in size and is a key factor in the brittle fracture mode.

Hull[6] listed the forces that develop in the crush zone during the fiber splaying mode as follows: compressive forces on the fronds and debris wedge, frictional forces as the fronds slide across the load platen, frictional forces between the debris wedge and the frond, frictional forces between lamina and fronds as they bend through different radii of

curvature, and hoop forces resulting from the inner and outer fibers resisting longitudinal crack propagation.

The energy dissipation methods for this failure mode have been summarized as follows: energy absorbed by longitudinal wall cracking, energy absorbed by delamination and formation of fronds, energy required for frond bending, energy required for fiber fracture, energy absorbed by various forms of friction listed above, and finally, other crack formation such as axial tube splitting.[21] It remains unclear as to the amount of energy absorbed by each dissipation method, although it has been shown that the various frictional effects account for up to half of the total energy absorbed for the fiber splaying failure mode.[23]

2.4.2.2 Fragmentation

Figure 2.5b) shows a typical cross section of a tube wall that has failed by fragmentation. The key characteristic of this failure mode is the formation of short (less than laminate thickness) interlaminar, intralaminar, and axial cracks.[20] These shorter cracks can be the result of either a matrix material with a higher maximum allowable shear stress or an interlocking fiber pattern, such as a triaxial braid. As crushing takes place compressive stresses build until failure occurs from shear stress on a plane inclined to the axis of the tube. This shear failure results from a mixture of fiber fracture, matrix fracture, buckling of the fibers, and interlaminar cracks.[21]

As a result of this shear failure, separated lamina pieces or wedge shaped fragments are forced to the inside and outside of the tube. Compressive stresses build in the remaining material of the tube wall until failure occurs and the process is repeated

again. It has been reported that this process can be essentially self-stabilizing, such that tubes with different initial conditions (e.g., trigger chamfer angles) will experience the same crush morphology once the initial crush zone has developed.[13]

Energy absorption for the fragmentation mode of failure comes primarily from fiber and matrix fracture. Since there are no fronds or other pieces to slide across one another or the load platen, frictional effects have been shown to contribute little to the SEA of tubes that fail by fragmentation.[24]

Typically, there is no debris wedge present in the fragmentation mode. Fractured pieces are cleared from the crush front and play no further part in energy absorption. It has been reported, however, that it is possible for fractured material to get caught in the crush front. This can result in a debris wedge that forms longer cracks and shifts the crush mode to a brittle fracture type mode of failure.[9]

2.4.2.3 Brittle Fracture

Figure 2.5c) shows a typical section of a tube wall that has failed by the brittle fracture mode. This failure mode is essentially a combination of the fiber splaying and fragmentation modes and has characteristics common to both. The longitudinal cracks that form are similar in length to the wall thickness and are long enough that fronds are formed as laminas are separated by cracks. However, the fronds are bent through a radius of curvature such that nearly all the fronds are fractured. Compressive stresses, especially in the central portion of the wall, are high enough that material fails in compression, forming a large debris wedge of pulverized material. This debris attempts to split the tube wall near the center and aids the formation of fronds.

Failure modes for brittle fracture include all of those associated with both fiber splaying and fragmentation modes of failure. Fiber and matrix fracture, friction, frond bending, and crack growth all contribute to the total energy absorbed by this failure mode.

2.4.2.4 Folding

This failure mode is analogous to the failure mode experienced by metal tubes when loaded in axial compression. It occurs when the stress in the tube wall is high enough that it buckles locally and forms a hinge. When the stress increases again to the required level, another hinge is formed below the previous, and the process is repeated. Each hinge will form a new fold until the entire tube length is collapsed. This failure morphology is also known as a concertina.

Tubes failing in a folding failure mode may experience significant amounts of interlaminar and longitudinal cracking during hinge formation. Fiber fracture, especially on the tension side of the hinge, may also occur.[20]

One advantage that the folding failure mode has over fiber splaying and fragmentation is that either the matrix or fibers remain intact to a large extent. This allows tube specimens to have postcrush integrity, which can be desirable for applications where energy absorbing structures would be required to remain attached following a crash. Tube specimens containing a portion of ductile fibers have been shown to exhibit this characteristic and hybrid composites are sometimes considered for this reason.[25]

Table 2.1 contains a summary of the four failure modes and their characteristics.

Table 2.1: Failure Mode Summary

	Fiber Splaying	Brittle Fracture	Fragmentation	Folding
Characteristics	Long axial cracks. Fronds are developed but do not fracture. Small debris wedge may be present.	Intermediate length axial cracks. Fronds develop and fracture. Large debris wedge present.	Short axial cracks. Sections of structure wall are sheared off. No debris wedge present.	Plastic hinges are formed locally. Inter / intralaminar cracking occurs near hinges.
Failure Mechanisms	Mode I and II fracture.	Mode I and II fracture. Fiber and matrix fracture.	Fiber and matrix fracture.	Buckling and plastic deformation. Some fiber and matrix fracture.
Energy Absorption Mechanisms	Friction, crack growth, frond bending.	Friction, fiber and matrix fracture, crack growth.	Fiber and matrix fracture.	Deformation, fiber and matrix fracture.

2.5 Selected Testing Results

To illustrate the energy absorption capability of composite tubes, testing results from selected authors are included in Table 2.2. Notable results include the high SEA values reported for thermoplastic materials, the maximum values of dynamic (>1 m/s displacement) SEA as compared to static (<1 x 10^{-3} m/s displacement) SEA, and the effect of cross sectional shape on reported SEA values. These trends are discussed in the following sections along with other variable effects.

There is significant variation of SEA values for metallic tubes in the literature (e.g., SEA values range from 16 to 75 kJ/kg for aluminum[4,7]). Maximum reported SEA values for metal tubes are included in Table 2.2 for reference.

Table 2.2: Selected Composite Tube Testing Results

SEA (kJ/kg)	Ref.	Fiber Type	Matrix Type	Layup / Architecture	Cross Section	Testing Rate
227	26	AS-4 carbon	PEEK	[±15]	circle	static
195	27	S2-glass	PEEK	[±10]	circle	static
188	28	T300 carbon	PEI	[±10]	circle	static
168	28	T800 carbon	PI	[±20]	circle	static
148	28	T650-35 carbon	PAS	[±15]	circle	static
125	9	AS-4 carbon	5245 epoxy	[0/±15]	circle	static
110	29	carbon/Kevlar	epoxy	$[(\pm 45)_f/(0/90)_f/0]_s$	circle	static
100	30	AS-4 carbon	PEEK	[±10]	circle	dynamic
95	12	T300 carbon	5208 epoxy	[0/±15]	circle	dynamic
90	31	T300 carbon	934 epoxy	[±45]	ellipse	static
88	32	AS-4 carbon	35016 epoxy	[0/±45]	cone	static
85	24	E-glass	HX205 epoxy	[±15]	circle	static
85	33	AS-4 carbon	LY1927 epoxy	knitted w/ axial	circle	static
84	34	T650-35 carbon	F584 epoxy	$[45_2/0_2/45]$	channel	static
78	35	E-glass	vinyl ester	csm	circle	static
77	36	E-glass	E53 epoxy	$[(0/90)_{f4}/0_4/(0/90)_{f4}]$	circle	static
75	37	E-glass	618 epoxy	[±75] wound	circle	dynamic
75	4	2024 Aluminum		-	circle	-
67	38	6061 Aluminum		-	circle	-
71	39	E-glass	polyester	csm	cone	static
67	40	E-glass	vinyl ester	[csm/0/csm]	circle	dynamic
67	34	T650-35 carbon	F584 epoxy	$[45_2/0_2/45]$	angle	static
67	4	4130 Steel		-	circle	-
65	7	E-glass	polyester	(0/90) cloth	circle	static
65	5	Kevlar	F161 epoxy	(0/90) cloth	circle	static
63	31	Kevlar	934 epoxy	[±45]	ellipse	static
63	42	carbon	epoxy	$[0_2/\pm 45_2/90_2]_s$	circle	dynamic
62	25	glass/carbon/Kevlar	vinyl ester	$(+45_g/-45_K/0_{cf})$	circle	static
62	43	E-glass	D331 epoxy	[±52] wound	circle	dynamic
60	44	AS-4 carbon	LY1927 epoxy	knitted w/ axial	circle	dynamic
60	40	E-glass	vinyl ester	[csm/0/csm]	square	dynamic
50	41	T300 carbon	epoxy	[0/±45] wound	circle	static
45	44	E-glass	LY1927 epoxy	knitted w/ axial	circle	dynamic
38	41	T300 carbon	epoxy	[0/±45] wound	square	static
35	38,4	1015 Steel		-	circle	-

2.6 Variables Affecting Energy Absorption in Composite Specimens

Due to the complex nature of failure in composite tube specimens, there are numerous factors that affect energy absorption values: fiber type, matrix type, fiber architecture, preform type, fiber volume fraction, specimen geometry, trigger type, strain rate, and loading surface roughness. In this section these parameter effects are described and related research is summarized.

2.6.1 Fiber Type

Farley[12] performed early studies on the effect of fiber type on energy absorption of composite tube specimens. Results showed for a $[0/\pm\theta]_3$ fiber orientation, carbon fiber produced higher SEA values than Kevlar or glass for $\theta < 30°$. However, all three fiber types had nearly equal SEA values for $\theta > 45°$. This result was attributed to the strain-to-failure difference between the fibers and matrix materials, with high strain fibers (Kevlar and glass) not being supported by the matrix during crushing at low θ values. However as θ increased, the angled fibers were able to support the 0° fibers and SEA values increased. Farley[9] expanded upon this research by testing two different carbon fiber types paired with low and high strain-to-failure matrices. It was found that higher strain-to-failure fibers and matrices resulted in higher SEA values due to reduced interlaminar cracking. It was recommended that the fiber strain-to-failure should be less than the matrix to avoid folding failure.

Thornton[5] reported carbon fiber had a higher SEA potential than E-glass for 0/90 woven fabric configurations. It was found that tubes reinforced with carbon fiber experienced more fragmentation in the crush zone while E-glass showed considerable

flexure. The increase in fiber fracture for carbon was likely the cause of higher SEA values. Ramakrishna[44] found that carbon fiber had higher SEA properties than E-glass for knitted fabric tubes as well. Ochelski and Gotowicki[36] investigated a large number of fiber architectures using single layers, fabrics, and mats and found that, on average, carbon fiber absorbed 20% more energy than glass fiber specimens of similar dimensions and constructions.

Schmuesser and Wickliffe[45] investigated $[0_2/\pm\theta]_s$ tubes fabricated from Kevlar, carbon fiber, and E-glass. It was found that for similar layups, the order of highest-to-lowest SEA was: carbon; Kevlar; E-glass. The SEA potential, found by varying the fiber angle θ, was also the highest for carbon fiber. Farley and Jones[31] reported similar results for tubular geometries with $[\pm 45]_n$ layups.

In summary, research results suggest that carbon fiber produces higher values of SEA than other candidate reinforcing fibers when comparing similar tube geometries with similar matrices. This result is attributed to carbon fiber's high tensile strength properties and relative low density when compared to E-glass. It is noted that Kevlar has tensile strength properties and density values similar to carbon fiber, although its low compressive strength and high strain-to-failure results in matrix failure and local buckling, reducing its SEA potential.[22]

Several authors have examined combining fibers in hybrid composite structures. Hybrid composites have been shown to maintain post-crush integrity and also have the potential for reduced costs. Farley[12] found that SEA levels for carbon/Kevlar hybrids were higher than carbon/E-glass using a $[0_{CF}/\pm 45_K]$ layup. However, it was noted that the SEA for hybrids were lower than for all-carbon tubes. Browne et al.[46] reported that

carbon fiber reinforced tubes had a higher SEA potential than a carbon/Kevlar/Nomex hybrid using a $[\pm 15]_n$ layup. Karbhari et al.[25] tested biaxial and triaxial braided layups of $[\pm 45]_n$ and $[0/\pm 45]_n$ and found the highest SEA using carbon/E-glass and carbon/Kevlar hybrids. Using the same inner diameter, wall thickness, and fiber volume fraction, Chui and Tsai[47] altered braiding and axial yarns for triaxial $[0/\pm 30]_n$ fabrics and found that pure carbon specimens and Kevlar/carbon specimens had nearly equal SEA values. These findings suggest that the potential of hybrid composite structures is promising, particularly when combining carbon axial fibers and Kevlar off-axis fibers.

In summary, the current published literature for composite tube crush testing indicates that the list of greatest to least SEA potential for fiber type is as follows: carbon ≥ hybrid > glass ≥ Kevlar. Hybrid composites, when correctly designed, can match or slightly exceed the performance of carbon fiber composites. Kevlar and glass have been shown to perform similarly, although the availability and low cost of glass fibers make them generally more attractive. The high SEA values for carbon fiber composites and carbon fiber-containing hybrids are attributed to carbon fiber's low density, high strength, and low maximum strain.

2.6.2 Matrix Type

The choice of matrix material has been shown to produce significant effects on the SEA of composite tube specimens. Berry et al.[48] showed that for thermosetting matrices, the highest-to-lowest order of SEA values obtained was: epoxy (EP); vinyl ester (VE); polyester (PE); phenolic (PN). Thornton et al.[49] and Thornton and Jeryan[50] presented similar results with a highest-to-lowest order of SEA values of: epoxy;

polyester; phenolic. Thornton[50] mentions that although it is not clear, the SEA does not appear to depend on fracture toughness of the matrix, but rather on the tensile strength and modulus. These results were verified by Warrior et al.,[51] which had the same ordering as Thornton et al.[49] Although good correlation was shown between matrix tensile strength and SEA, a better correlation was shown using matrix compressive strength.

Farley et al.[9] investigated the effects of matrix strain-to-failure on SEA using thermosetting matrices. Results showed that as the strain-to-failure of the matrix increased, the number of interlaminar cracks decreased and resulted in higher SEA values. Since the fracture toughness (G_{1C}) of thermosetting matrices generally increases with the strain-to-failure,[52-56] such increases would reduce the interlaminar cracking during fiber splaying and brittle fracture modes.

Ramakrishna et al.[28] performed tube crush tests using thermoplastic matrices and found that the order of highest-to-lowest SEA values was: polyetheretherketone (PEEK); polyethermide (PEI); polyimide (PI); polyarysulfone (PAS). This hierarchy was attributed to the fracture toughness of the thermoplastic matrices by noting that G_{1C} of PEEK is much higher than that of PEI or PI. It was also noted, however, that PEEK samples had a high number of fiber fractures and that PEEK has a crystalline structure (PEI and PI have an amorphous structure) and may be able to bond better to fibers.[57] Hamada and Coppola[58] compared carbon fiber/PEEK and carbon fiber/epoxy tubes and found that when stable crushing occurred, SEA values were much higher for tubes produced using PEEK.

Beyond choosing the matrix material with the highest SEA, it can be advantageous to increase the SEA of matrices that have other desirable properties (e.g., low cost or ease of manufacturing). Several studies have examined matrix toughening strategies or the use of interleaves. Warrior et al.[59] studied the effect of varying amounts of thermoplastic additive to increase fracture toughness of vinyl ester and polyester resins. It was found that even though fracture toughness varied 30% for thermoplastic quantities of 2% to 10% by matrix mass, the SEA values remained nearly constant. Yuan et al.[42] found that for carbon fiber/epoxy prepreg tubes, an interleave of polyethelene terephthalate (PET) increased SEA values. This increase was significant for layups containing ±45° layers. Warrior et al.[59] found that urethane interleaves between continuous strand mat or 0°/90° no-crimp fabric reduced the SEA values even though they significantly increased the fracture toughness. This result was attributed to the reduced coefficient of friction of the interleaf where axial splitting was occurring. The discrepancies in the studies above could be due to the differences in interleaf type and fiber architecture.

In general, thermoplastic matrices have been found to produce higher SEA values than thermosetting matrices. This result should be used with caution, however, as dynamic SEA values for thermoplastics have been shown to decrease by more than a factor of two when compared to quasi-static values.[30] For thermosetting matrices it can be concluded that for similar layups, the order for highest-to-lowest SEA values are: epoxy; vinyl ester; polyester. The matrix property that influences SEA values the most is difficult to determine. It is possible that the resulting failure mode plays an important factor. Fiber splaying, with Mode I and II crack growth as a dominant energy absorption

mechanism, may be influenced more by the fracture toughness. Fragmentation, with fracture as the dominant energy absorption mechanism, may be influenced more by the compressive and shear strengths of the matrix.

2.6.3 Fiber Architecture

Several common layups for tubular specimens have been investigated extensively. These layups are popular because they can be manufactured easily by methods such as roll-wrapping or filament winding. These common layups include [0/90], [0/±θ], and [±θ]. Research results of Thornton[17] have shown that tubes having fiber orientations in the 0° (axial direction) and 90° (hoop direction) have potential for high SEA values. Note that [0/90] layups can be produced by wrapping or by using (0/90) fabric. Thornton tested circular and square tubes of carbon fiber, E-glass, and Kevlar having various relative densities.[17] Results show that $[0/90]_n$ layups had higher SEA values than $[\pm 45]_n$ layups for all fiber types and relative densities. The differences in values were substantial in all cases, ranging from 15 – 40% depending on fiber type. Similarly, Hull[60] found a decrease of ~30% in SEA value when comparing filament wound E-glass $[\pm 55]_n$ to rolled E-glass using $[(0/90)_f]_n$ fabric.

Stacking sequence has been shown to be important for [0/90] layups. Farley[12] found that for a tube to exhibit stable crush, 90° inner and outer layers should be present. Hull[60] noted an unstable failure mode when testing pultruded tubes with 0° outer plies. Hull[6] also noted that the highest SEA values were found when placing 90° plies on the outside and inside symmetrically, or on the outside entirely, depending on load rate. In all the cases above, outer 0° plies tended to delaminate and buckle, resulting in a barreling

failure mode. As a result, 90° or angle plies should be placed on the inside and outside of structures to avoid this type of failure.

Hull[6] investigated the effect of the ratio of hoop (90°) to axial (0°) fibers on the overall SEA of glass fabric rolled tubes. It was found that as the ratio changed from 8.5:1 to 1:8.5, the failure mode and energy absorption changed drastically. SEA values increased as the amount of axial fibers increased until a ratio of 1:4. At this point, an increase in axial fibers did not result in higher SEA values due to lower hoop constraints and little to no fiber fracture.

[0/±θ] layups are commonly produced by roll wrapping or using triaxial braided fabric. Shmuesser[45] performed tests on $[0_2/\pm\theta]_s$ tubes with circular cross sections and θ values between 30° and 90°. It was found that for glass/epoxy tubes, the highest SEA value was for $[0_2/90_2]_s$. For carbon/epoxy, the $[0_2/\pm60]_s$ layup performed the best, although the SEA of the [0/90] layup was only 3% below this. Kevlar also showed the highest SEA value at θ = 60°. Okano et al.[61] showed that for triaxial braided carbon fiber, SEA values increased as the braid angle increased from 30° to 60°. Similarly, Johnson et al.[62] showed a higher braid angle (53° compared to 30°) increased the SEA of hourglass shaped rails.

Farley[12,63] reported findings for E-glass and Kevlar tubes with [0/±θ] layups made from roll wrapping. The highest SEA values were found at 75° and 90° for E-glass and Kevlar, respectively. For carbon fiber, however, the highest SEA values occurred when θ equaled 15°. This result was attributed to a reduction in stiffness of the specimen in the fiber direction as θ increases. It should be noted that with the layup used, there were

twice as many θ plies as 0° plies. Differences in results between this study and ones using $[0_2/\pm\theta]_s$ layups should be expected.

Hamada et al.[28,64] found results similar to Farley's with carbon fiber/thermoplastic matrices including PEEK, PEI, PI, and PAS using $[0/\pm\theta]_n$ layups. The highest SEA values occurred for θ equal to 10° or 15° for PEEK, PEI, and PAS. For PI the highest values of SEA occurred near θ equal to 20°. For θ values higher than 20° many of the tubes experienced non-progressive failure due to instability.

Helical filament winding or biaxial braided fabrics result in [±θ] layups. Kindervater[18] found that the general trend was for SEA to increase with increasing θ for angles of 15° to 75° for E-glass, carbon fiber, and Kevlar materials [14]. Hull[6] and Song et al.[37] reported similar findings for filament wound E-glass / epoxy tubes. Farley,[9] however, reported a decrease in SEA with increasing θ for roll-wrapped tubes using T300 and AS-4 carbon fiber.

2.6.4 Fiber Preform Type

Several studies have investigated the effects of using different fiber forms to manufacture composite tube specimens. Several fiber forms have been shown to have high SEA potential while others, even though they have relatively low values, are still viable due to cost and manufacturing considerations. Woven fabric, either in twill or plain weave forms, has been used by many authors due to its ease of manufacturing.[5,6,7,51,65,66] Kindervater[18] reported that tubes containing carbon fiber woven fabric generally had lower SEA than those with unidirectional prepreg or tape.

Thornton[17] was able to increase the SEA of circular and square tubes made from (0/90) fabric by replacing several of the inner laminas with 0° unidirectional tape layers.

Mamalis et al.[67,68] performed testing on chopped mat/polyester tube specimens, noting their low cost. It was found that chopped mat tubes outperformed pultruded tubes as well as tubes made from 0° and 90° unidirectional layers with chopped mat. Although not producing SEA values as high as other glass fiber forms, chopped mat typically is available at a lower cost.

In recent years, several authors have investigated the SEA properties of continuous strand mats (CSM) made from glass fibers and polyester or vinyl ester resin.[35,36,69] This preform is promising due to its high SEA values, which are reportedly comparable to E-glass/epoxy prepreg tubes.

Pultruded tubes are relatively inexpensive and can be produced in a continuous process that makes this an attractive technique for large volume productions. The most common pultruded layups include CSM layers interspersed with 0° unidirectional layers, although many other possibilities exist. Pultruded tubes have produced similar or slightly lower SEA values when compared to other glass/polyester tubes.[40,67,70] However, the SEA values are much lower than glass/epoxy tubes.

2.6.5 Fiber Volume Fraction

Research into the effect of fiber volume fraction, V_f, on SEA values has traditionally focused on chopped or knitted constructions where V_f values are less than 0.5. Ramakrishna et al.[33,44] varied the fiber volume fraction of carbon fiber/epoxy knitted fabric tubes with and without inlay fibers from 0.10 to 0.33 and found that SEA increased

over this range. Karbhari[25] reported similar findings with four-layer biaxial braided tubes, noting that SEA increased as fiber volume increased from 0.22 to 0.42. Finally, Snowdon and Hull[71] showed that SEA increased for sheet molding compounds (SMC) as the volume fraction increased from 0.13 to 0.18.

These research results indicate that for fiber preforms with values of V_f less than 0.5, increases in V_f produce increases in the SEA values for composite tubes. However, a very high V_f can result in reduced SEA properties. Farley[19] varied the fiber volume fraction of prepreg layups and found that, in general, SEA values decreased as V_f increased above 60%. This was due to reduced interlaminar strength as the volume of the resin between fibers decreased.[19]

2.6.6 Tube Specimen Geometry

Thornton[5,17] considered the role of thickness-to-diameter (t/D) ratios in the crush of tubular specimens. Results showed that for [0/90] and [±45] layups using glass, carbon, and Kevlar fiber, SEA values obtained from tube specimens were essentially independent of tube dimensions. However, other authors have reported very different results. Farley[72] reported that the SEA of carbon fiber/epoxy [±45] tubes was a nonlinear function of the *t/D* ratio, with increasing SEA for increasing *t/D* ratios. Mamalis[8] reported increases in SEA with increases in *t/D* ratios for circular specimens of glass CSM and woven fabric. Hamada[73] reported similar results with carbon fiber/PEEK tubes, but only up to a certain value of *t/D*. This result was attributed to thick walls having larger sections of wall fracturing (approaching unstable failure). These results suggest that SEA

values increase as *t/D* ratios increase as long as unstable type failure mechanisms are avoided.

Elgalai and Hamouda[74] investigated the effect of length-to-diameter (*L/D*) ratios of composite tube specimens on SEA values. Results showed that the optimal *L/D* ratio for woven glass fabric tubes was approximately 5:1. However, failure modes of other *L/D* ratios did not exhibit completely progressive failure. Variations in SEA values for *L/D* ratios between 2:1 and 6:1 were in the range of 20%. This finding suggests a slight dependence of SEA on the *L/D* ratio. However, consideration of the resulting failure modes suggests that as long as continuously stable failure is occurring, the resulting SEA values are relatively independent of *L/D* and *L/S* ratios.

The energy absorption of metallic structures can remain constant if cross sections are geometrically scaled (constant *t/D* ratio or relative density, ϕ). Several studies have investigated geometric scaling of energy absorption in composite structures using tube specimens. Farley[72] found that for Kevlar tubes, the SEA did remain nearly constant for geometrically scaled cross sections. This result was attributed to Kevlar and metals both failing in a folding mode. It was shown for carbon fiber, however, that SEA values were not constant as the tube geometry was scaled. Hamada et al.[73] reported similar results for carbon fiber/PEEK tubes. SEA values were found to be a function of the actual tube diameter *D* in addition to the *t/D* ratio. These results suggest that the SEA does not remain constant when geometrically scaling cross sections of composite tubes exhibiting non-folding failure modes.

The effect of cross sectional shape on the energy absorption of composite tubes has been investigated by many researchers. Thornton[5,17] observed that cross sectional

shapes with planar sections (squares and rectangles) are less effective in absorbing energy than circular shapes. The ranking for energy absorption was given as circle > square > rectangle. Other authors have made this observation for filament wound specimens,[41] continuous filament random mat specimens,[69] and fabric specimens.[75] Yang[76] performed tests with square specimens using several corner radius sizes and found that the SEA increased as the corner radius increased. This result may be viewed as the SEA increasing as the square shape more closely approaches a circle.

Farley and Jones[31] reported on near-elliptical cross sections and found that as the included angle decreased (a/b of the ellipse increased), SEA values increased from 10-30% depending on *t/D* ratio. This increase in SEA was attributed to the percentage of the area near the corners of the ellipse. Feraboli[77] tested various angle sections and found that elements containing a corner with small plane sections absorbed significantly more energy than those with larger plane sections. The local tearing that occurred at the corner was thought to cause this increase in energy absorption. Kinderavter[18] and Bulokbasi et al.[34] also tested channel and angle sections. Results showed that channel sections, having one additional corner, absorbed more energy than angle sections.

Tapered composite tubes of circular, square, and elliptical cross section have been investigated. Pafitis and Hull[78] and Jacob and Fellers[79] showed that the load versus displacement curves of conical shaped composite tubes can be tailored as linear or exponential, for example, by altering the cone dimensions. Cones have also been shown to absorb more energy than constant cross sections in off-axis testing.[32] However, Ochelski and Gotowicki,[36] Mamalis,[67] Hannapel and Yuan,[39] and Fleming and Vizzini[32] all found that SEA values decrease as cone angle increased, limiting the effectiveness of

large angles. Ochelski and Gotowicki[36] attributed this finding to the increased bending moment that is produced in laminas as the cone angle increases.

In summary, research results suggest that the SEA of tube cross sections is greatest for circles, followed by squares, and finally by rectangles. Shapes containing corners have been shown to have high energy absorption values and various angle sections typically rank between circles and squares in terms of SEA. However, since energy absorbing components typically also need to be structural components sizes and shapes may be driven by design requirements. In this case it would be important to optimize the geometric parameters that can be controlled such as the relative size of planar sections and *t/D* and *t/S* ratios.

2.6.7 Trigger Type

Triggers are geometric modifications made to one or both ends of the tube that act as stress concentrations to promote local failure. Initially developed for metallic tubes, they have been shown to reduce peak loads and promote progressive failure in composite tubes by encouraging crushing at the reduced cross sectional area of the trigger.[5] Some common types of triggers are single and double bevels, notches, tulips, holes, and ply drops[15,80] (Figure 2.6).

Single bevel triggers are common due to their simplicity. Sigalas and Hull[13] investigated the bevel angle (measured from the axis) on the initial load versus displacement curve of woven glass fabric/epoxy tubes. For this material, which failed by fragmentation, the chamfer angle played a large role in the initial slope of the loading curve but did not play a role in the mean load during stable crushing.

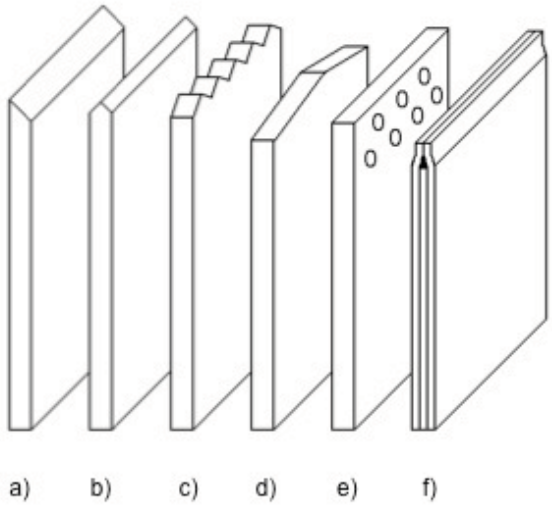

Figure 2.6: Trigger types: (a) single bevel, (b) double bevel, (c) notch, (d) tulip, (e) hole, and (f) ply drop.

Thornton[81] and Sigalas et al.[13] compared single and double bevels to tulip triggers in circular and square cross sections. Both authors reported that there was an increase in SEA when using the tulip trigger. Sigalas[13] noted that for square specimens with bevel triggers there appeared to be a larger number of deep cracks into the length of the tube that resulted in lower SEA values. Czaplicki[14,15] investigated the SEA of square tubes with bevel, tulip, and various hole triggers. A 20% increase in mean load for stable failure was found when using a tulip trigger and several hole trigger configurations. It was noted that tubes that failed catastrophically with a bevel trigger sometimes failed stably with a tulip trigger or hole trigger. The author noted that triggering is both structural and material dependant, and thus these results may not apply universally.

Thuis and Metz[29] investigated several ply drop trigger options. They found that the manner in which plies were dropped affected the failure mode, peak load, and overall

SEA of specimens. The ply drop trigger that provided the highest SEA closely resembled the geometry of a single bevel.

Trigger mechanisms have been shown to be less important for materials that fail in the fiber buckling mode. Thornton[17] noted that for Kevlar tubes, bevel triggers are unsuitable and proposed that a trigger for metal tubes, such as a crimp, be used.

Triggers that are separate from the composite tube have been considered. These triggers can be advantageous in that they provide a means of attachment to larger structures. The most common is a radiused plug with a cap. This type of trigger forces a fiber splaying failure mode and results in the formation of long axial cracks (Figure 2.7). These cracks separate the tube wall into what are referred to as pedals. Browne and Johnson[46] reported a loss in SEA for roll-wrapped carbon fiber and E-glass fabric tubes when comparing 45° bevels to internal plug triggers. The forced failure mode that accompanied the plug was cited as a possible reason. Abdel-Haq and Newez[70] found that as the plug radius decreased, SEA increased for pultruded glass/polyester tubes. Warrior[69] found that for CSM circular and square tubes, the SEA was modestly higher for a 0 mm plug radius (sharp corner) than for a 45° bevel alone.

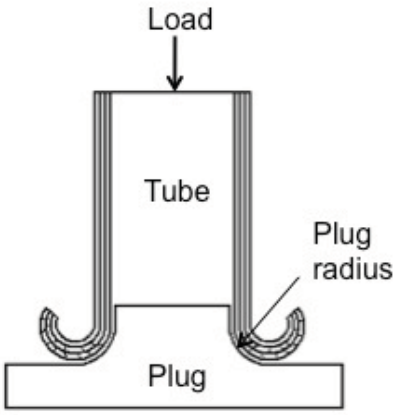

Figure 2.7: Composite tube crushed on an internal trigger

In summary, the use of a triggering mechanism is an important consideration for composite tube crush testing. The single bevel is the most popular trigger and appears to work well for the majority of tube geometries and materials. However, for tubes with planar sections, tulip and hole triggers have been shown to result in lower peak loads and higher energy absorption values. Internal plug triggers with small radii have been shown to be advantageous when using materials with lower in-plane properties such as CSM. It should be cautioned that triggering effects are a function of material, geometry, and other parameters and so it is difficult to apply any of these findings universally.

2.6.8 Strain Rate

Currently there is considerable confusion in the literature concerning the effect of loading speed and strain rate on the energy absorption of composite tubes. Thornton[5] found near rate independence of SEA for T300 carbon/epoxy and E-glass/epoxy fabric tubes for test speeds of 4×10^{-5} m/s to 8.5 m/s. It was noted that there was no tendency for unstable collapse and the only change that occurred with load rate was a larger serration of the load versus displacement curve. Thornton[40] reported that for pultruded E-glass/polyester CSM tubes SEA increased up to 20% with load rate from 2.1×10^{-4} m/s to 14 m/s. For similar architectures using vinyl ester resin, SEA values decreased approximately 10%. This decrease was attributed to a change in crushing mode, with fewer fiber fractures occurring at higher load rates for the vinyl ester resin.

Hull[7] found the SEA of E-glass/polyester and epoxy tubes using wound and fabric forms to be nearly independent of load rate. SEA was found to vary less than 10% for speeds of 4 mm/s to 4 m/s. Hull[6] later reported that for (0/90) rolled E-glass/polyester

tubes, SEA variation with load rate was dependent on the percentage of fibers in the axial direction. A marked change in crushing mode was noted for fiber arrangements with a high proportion of axial fibers. Changes in friction forces with increased load rate were thought to be responsible, due to fronds sliding against the loading platen during the fiber-splaying mode.

Berry and Hull[65] tested roll-wrapped glass/epoxy fabric tubes at rates of 1.67×10^{-7} to 10 m/s. SEA values more than doubled over the increasing loading rates used for testing and were found to increase nearly linearly with the log of testing speed. A shift in matrix failure from ductile to brittle was observed at higher loading rates.

Farley[12] investigated carbon/epoxy, Kevlar/epoxy, and E-glass/epoxy tubes with [0/±θ] and [±θ] layups and found that failure modes and energy absorption were essentially independent of load rate. Farley[63] later reported on [0/±θ] and [±θ] tubes of carbon/epoxy, glass/epoxy, and Kevlar/epoxy, finding that the SEA of the [0/±θ] layup using glass and carbon fiber was rate independent. This result was attributed to the energy absorption being primarily produced by fiber failure, which is not known to be strain rate sensitive. However, the SEA of tubes with the [±θ] layup was found to increase up to 35% with increasing load rate. The matrix material, known to be strain rate sensitive, was thought to have more influence due to the combination of fragmentation/fiber splaying mode that occurred. Both layups using Kevlar fibers showed increases in SEA values of between 20-45% with increasing load rate. This result was linked to the polymeric nature of Kevlar and its inherent strain rate sensitivity.

Kindervater[82] tested carbon fiber/epoxy tubes with [±θ] architecture manufactured by the filament winding technique and found that the trend was for slightly lower SEA

values with increased load rate. This finding was not universal, and the author comments that the phenomena that occur are not well understood. Schmueser and Wickliffe[45] tested [0/±45] layup tubes with carbon, E-glass, and Kevlar fibers and an epoxy matrix. They reported that static crush results could overestimate the dynamic energy absorption of all materials by up to 30%. They found similar failure modes for testing speeds of 10 mm/min and 5 m/s, and noted the difference could be due to fracture toughness sensitivity of the composites at high strain rates.

Mamalis et al. performed several investigations into the response of thin walled tubes under static and dynamic loading. The first results were for circular tubes made from E-glass/polyester boat fabric tested at speeds of 1.14, 11.4, and 114 mm/sec.[8] When comparing stable collapse of tubes, it was found that the energy absorbed decreased slightly as the load rate increased. Later, when testing circular and square tubes of E-glass/vinyl ester that contained 0°, 90°, and chopped mat layers it was found that energy absorption was nearly unchanged for load rates of 2.1×10^{-4} m/s to 22 m/s.[67] Similar results were reported for pultruded square tubes with 0° and chopped mat layers with the same constituents. For chopped E-glass/polyester tubes, it was found that the SEA generally decreased with increasing load rate for circular and square tubes by up to 10%. This result was believed to be due to the polyester resin shattering during impact testing. For square tubes, it was also noted that the debris wedge was much smaller during impact testing, possibly reducing frictional effects. Similar findings were reported for chopped E-glass/polyester with testing speeds up to 10 m/s.[68] Finally, square tubes made from carbon fabric/epoxy were investigated at load rates of 7 mm/min and 5.4 m/s.[83] A trigger was not used on the tubes and there was a tendency for dynamically loaded specimens to

not crush progressively. Due to this, these findings are difficult to apply. It was found that SEA decreased with load rate by an average of approximately 50%.

Ramakrishna and Hamada[44] tested knitted E-glass and carbon fiber tubes with an epoxy resin at load rates of 0.001 m/s and 13 m/s. Energy absorption of both fibers decreased with load rate by up to 25%. In a separate study it was found that energy absorption of glass fabric tubes increased by 5 to 15% depending on the fiber treatment with test speeds of 0.001 m/s and 8.5 m/s.[84] Increases in SEA were thought to be the result of failure mode shifts from fragmentation to mixed fragmentation/splaying mode. Tests performed by the same authors on [0], [±5], and [±10] carbon fiber/PEEK composite tubes at 1.67×10^{-5} m/s and 8.5 m/s produced almost 50% decrease in the SEA as load rate increased.[30] A failure mode shift from fiber splaying to brittle fracture was noted and thought to be due to the reduced fracture toughness of PEEK at high strain rates.

Arnaud and Hamelin[43] tested filament wound [±45] and woven [±52] tubes using E-glass and carbon fiber with vinyl ester and epoxy matrices. Tubes were tested at load rates up to 16 m/s. Results showed that vinyl ester tubes had a slight decrease in SEA with load rate while epoxy tubes experienced a slight increase. The author notes large variability in the data and that the changes were not significant in either case.

Karbhari and Haller[85] tested hybrid biaxial and triaxial fabric tubes with various layers of E-glass, carbon, and Kevlar fiber with vinyl ester resin. SEA increased from 5% to 30% with load rate for nearly all fibers and ply orientations. A change in crush morphology was noted for many specimen groups, including an increased number of fronds during the fiber splaying failure mode or increased fragmentation.

Song and Du[37] investigated [±θ] E-glass/epoxy tubes manufactured by filament winding and loaded at 8.3 x 10^{-5} m/s and 6 m/s. They reported a shift in rate dependence at a fiber angle θ of approximately 35°. Fibers angles less than this value experienced decreases in SEA with load rate whereas fiber angles above experienced increases. It was hypothesized that since the [±15] and [±30] layups failed in the fiber splaying mode, the rate sensitivity of matrix cracking caused the decrease in SEA. For fiber angles θ of 45°, 60° and 75°, fragmentation occurred.

Brimhall[86] tested square carbon fiber/vinyl ester tubes using a [0/±45] triaxial braided architecture at load rates of up to 5 m/s. The SEA decreased approximately 22% with increasing load rate. The tubes were tested using an internal plug trigger, and similar failure modes were observed for both loading rates. By utilizing a roller testing jig, sliding friction was found to be nearly entirely responsible for this loss in energy. Warrior[69] reported similar findings testing circular tubes using E-glass CSM and polyester resin. Dynamic SEA was found to be from 6% to 50% less than static values depending on the plug trigger radius.

Brighton et al.[66] reported on carbon/epoxy and glass/polypropylene tubes produced by a short-cycle manufacturing process. Both types of materials consisted of (0/90) fabric. It was found that the SEA for carbon/epoxy tubes decreased by 15% to 22%, depending on trigger geometry, for loading rates of 10 mm/min to 4 m/s. This decrease in SEA with increasing loading rate was thought to result from the larger radius of the fronds, which resulted in less fiber fracture. The SEA values of the glass/polypropylene tubes were found to vary by 40% over the loading rates tested,

initially increasing and then decreasing. Failure modes shifted dramatically across the range of loading rates, from folding to an inversion type failure.

In summary, there is no current consensus on the strain rate effect on SEA in composite tubes. A common belief is that energy absorption will be a function of strain rate if the resulting failure mechanisms are also a function of strain rate. Since different fiber types, matrix types, architectures, and geometries all have different failure responses, strain rate effects are difficult to summarize universally.

2.6.9 Loading Surface Roughness

Farley and Wolterman[24] investigated the effect of platen roughness on the SEA of carbon fiber/epoxy and E-glass/epoxy tubes. Tubes were constructed of either [0/±θ] or [±θ] layups and tested at 5 mm/min. Two plate roughness values were tested, 12 μm (rough) and 0.3μm (smooth). The only effect of loading surface roughness on SEA was found for tubes that failed in the fiber splaying mode. For such tubes, the variation in SEA was found to be dependent on the fiber and matrix strain used in the specimen.

Fairfull and Hull[23] tested E-glass/epoxy fabric at 20mm/min using four values of surfaces roughness. They found that by reducing the coefficient of friction, a 20% reduction in crush load was observed. It was concluded that even for relatively smooth plates various frictional effects accounted for nearly 50% of the energy absorbed. Brimhall[86] found that when testing carbon fiber/vinyl ester tubes using an internal plug trigger, approximately 35% of the energy absorbed was due to sliding friction against the plug.

The research reviewed shows that friction between the specimen and the loading surface can have a significant effect on the total energy absorption. The SEA of tubes that fail in the fiber splaying mode appear to be more affected by surface roughness than those that fail in fragmentation mode.

2.7 Summary

This paper has presented a current understanding of composite tube testing, which remains a popular means of assessing the energy absorption properties of composite materials. Energy absorbing mechanisms that occur during crush tests are functions of many variables including material type, fiber architecture, tube geometry, and strain rate. The effects of some of these variables are well understood while others, notably strain rate, lack a consensus.

Composite materials will grow more prevalent in the primary structures of vehicles, thus, understanding their crashworthiness characteristics is essential. Further research is necessary to fully understand variable effects on energy absorption properties and to also develop analytical tools that will aid in the design of crashworthiness structures.

2.8 References

1. U.S. Department of Transportation, *Federal Motor Vehicle Safety Standards and Regulations*, no. 201-224 (Washington, DC, 1998).

2. U.S. Department of Defense, *Light Fixed and Rotary-Wing Aircraft Crash Resistance*, MIL-STD-1290A (Washington, DC, 1988).

3. Railtrack, *Structural Requirements for Railway Vehicles*, Railway Group Standards GM/RT 2100 (July 1994).

4. C.L. Magee and P.H. Thornton, "Design Considerations in Energy Absorption by Structural Collapse," *SAE Prepr*, n 780434, 1978, February 27 – March 3.

5. P.H. Thornton, "Energy Absorption in Composite Structures," *Journal of Composite Materials* 13 (1979), 247-62.

6. D. Hull, "A Unified Approach to Progressive Crushing of Fiber-Reinforced Composite Tubes," *Composite Science and Technology* 40 (1991), 377-421.

7. D. Hull, "Energy Absorption of Composite Materials under Crash Conditions," *Progress in Science and Engineering of Composites* (1982), T. Hayashi, K. Kawate and S. Umekawa, (eds), 861-870.

8. A.G. Mamalis and D.E. Manolakos, "Crashworthy Behavior of Thin-Walled Tubes of Fibreglass Composite Materials Subjected to Axial Loading," *Journal of Composite Materials* 24 (1990), 72-91.

9. G.L. Farley, "Effect of Fiber and Matrix Maximum Strain on the Energy Absorption of Composite Materials," *Journal of Composite Materials* 20 (1985), 322-334.

10. T.J. Brimhall, "Friction Energy Absorption in Fiber Reinforced Composites," Thesis (2005), Michigan State University.

11. G.C. Jacob, "Automotive Crashworthiness of Adhesively Bonded Carbon Fiber Polymer Composite Structures," Thesis (2006), University of Tennessee.

12. G.L. Farley, "Energy Absorption of Composite Materials," *Journal of Composite Materials* 17 (1983), 267-279.

13. I. Sigalas, M. Kumosa and D. Hull, "Trigger Mechanisms in Energy Absorbing Glass Cloth/Epoxy Tubes," *Composites Science and Technology* 40 (1991), 265-287.

14. M.J. Czaplicki, R.E. Robertson and P.H. Thornton, "Comparison of Bevel Tulip Triggered Pultruded Tubes For Energy Absorption," *Composites science and Technology* 40 (1990), 31-46.

15. M.J. Czaplicki, P.H. Thornton and R.E. Robertson, "Collapse Triggering of Polymer Composite Energy Absorbing Structures," *How to Apply Advanced Composites Technology* (American Society for Metals, 1988), 39-46.

16. Correspondence with Graham Barnes, Engenuity, Ltd.

17. P.H. Thornton and P.J. Edwards, "Energy Absorption in Composite Materials," *Journal of Composite Materials* 16 (1982), 521-545.

18. C.M. Kindervater, "Crash Impact Behavior and Energy Absorbing Capability of Composite Structural Elements," *30th International National SAMPE Symposium* (1985), March 19-21.

19. G.L. Farley, "Energy Absorption of Composite Material and Structure," *43rd American Helicopter Society Annual Forum* (1987), 613-627.

20. G.L. Farley and R.M. Jones, "Crushing Characteristics of Continuous Fiber-Reinforced Composite Tubes," *Journal of Composite Materials* 26 (1992) 37-50.

21. S. Ramakrishna and H. Hamada, "Energy Absorption Characteristics of Crash Worthy Structural Composite Materials," *Key Engineering Materials* 141-143 (1998), 585-620.

22. J.J. Carruthers, A.P. Kettle and A.M. Robinson, "Energy Absorption Capability and Crashworthiness of Composite Material Structures: A Review," *Applied Mechanics Review* 51, no. 10 (1998), 635-649.

23. A.H. Fairfull and D. Hull, "Energy Absorption of Polymer Matrix Composite Structures: Frictional Effects," *Structural Failure* (1988), T Wierzbicki and N Jones (eds), 255-279.

24. G.L. Farley, R.L. Wolterman and J.M. Kennedy, "Effects of Crushing Surface Roughness on the Crushing Characteristics of Composite Tubes," *Journal of the American Helicopter Society* (July 1992), 53-60.

25. V.M. Karbhari , P.J. Falzon and I. Herzberg, "Energy Absorption Characteristics of Hybrid Braided Composite Tubes," *Journal of Composite Materials* 31, no. 12 (1997), 1164-1186.

26. H. Hamada, S. Ramakrishna and Z. Maekawa, "Effect of Cooling Rate on the Energy Absorption Capability of Carbon Fibre / PEEK Composite Tubes," *Polymers and Polymer Composites* 3, no. 2 (1995), 99-104.

27. H. Hamada and S. Ramakrishna, "Effect of Fiber Material on the Energy Absorption Behavior of Thermoplastic Composite Tubes," *Journal of Thermoplastic Composite Materials* 9 (July 1996), 259-279.

28. S. Ramkrishna, H. Hamada and Z. Maekawa, "Energy Absorption Behavior of Carbon-Reinforced Thermoplastic Composite Tubes," *Journal of Thermoplastic Composite Materials* 8 (1995), 323-344.

29. H.G. Thuis and V.H. Metz, "The Influence of Trigger Configurations and Laminate Lay-up on the Failure Mode of Composite Crush Cylinders," *Composite Structures* 28 (1994), 131-137.

30. H. Hamada and S. Ramakrishna, "Comparison of Static and Impact Energy Absorption of Carbon Fiber / PEEK Composite Tubes," *Composite Materials: Testing and Design 12th ed* (1994), R.B. Deo and C.R. Saff (eds), 182-198.

31. G.L. Farley and R.M. Jones, "Crushing Characteristics of Composite Tubes With Near Elliptical Cross Sections," *Journal of Composite Materials* 26, no. 12 (1992), 1741-1751.

32. D.C. Fleming and A.J. Vizzini, "Tapered Geometries for Improved Crashworthiness Under Side Loads," *Journal of the American Helicopter Society* (January 1993), 38-44.

33. S. Ramakrishna and D. Hull, "Energy Absorption Capability of Epoxy Composite Tubes With Knitted Carbon Fibre Fabric Reinforcement," *Composites Science and Technology* 49 (1993), 349-356.

34. A.O. Bolukbasi and D.H. Laananen, "Energy Absorption in Composite Stiffeners," *Composites* 26 (1995), 291-301.

35. T.A. Turner, F. Robitaille, N.A. Warrior, C.D. Rudd and E.J. Cooper, "Effect of Resin Formulation on Crash Energy Absorbing Composite Structures Made by RTM," *Plastics, Rubber and Composites* 31, no. 2 (2002), 49-57.

36. S. Ochelski and P. Gotowicki, "Experimental Assessment of Energy Absorption Capability of Carbon-Epoxy and Glass-Epoxy Composites," *Composite Structures* 87 (2009), 215-224.

37. H.W. Song, X. Du and G. Zhao, "Energy Absorption Behavior of Double-Chamfer Triggered Glass / Epoxy Circular Tubes," *Journal of Composite Materials* 36, no. 18 (2002), 2183-2199.

38. H. Saito, E.C. Chirwa, R. Inai and H. Hamada, "Energy Absorption of Braiding Pultrusion Process Composite Rods," *Composite Structures* 55 (2002), 407-417.

39. F.W. Hannapel, Y.B. Yuan, G.L. Viegelahn and C.D. Martin, "Crashworthy Characteristics of Fiberglass / Polyester Frusta Under Quasi-Static Axial Loading," *Advanced Materials: New Developments and Applications Conference Proceedings* (1991), 469-479.

40. P.H. Thornton, "The Crush Behavior of Pultruded Tubes at High Strain Rates," *Journal of Composite Materials* 24 (1990), 594-615.

41. M.R. Schultz and M.W. Hyer, "Static Energy Absorption Capability of Graphite-Epoxy Tubes," *Journal of Composite Materials* 35, no. 19 (2001), 1747-1761.

42. Q. Yuan, S. Kerth, J. Karger-Kocsis and K. Friedrich, "Crash and Energy Absorption Behavior of Interleaved Carbon-Fibre-Reinforced Epoxy Tubes," *Journal of Materials Science Letters* 16, no. 22 (1997), 1793-1796.

43. P. Arnaud and P. Hamelin, "Dynamic Characterization of Structures: A Study of Energy Absorption in Composite Structures," *Composites Science and Technology* 58 (1997), 709-715.

44. S. Ramakrishna, "Energy Absorption Characteristics of Knitted Fabric Reinforced Epoxy Composite Tubes," *Journal of Reinforced Plastics of Composites* 14 (1995), 1121-1141.

45. D.W. Schmueser and L.E. Wickliffe, "Impact Energy Absorption of Continuous Fiber Composite Tubes," *Journal or Engineering Materials Technology* 109 (1987), 72-77.

46. A.L. Browne and N.L. Johnson, "Dynamic Axial Crush Tests of Roll Wrapped Composite Tubes: Plug vs. Non-Plug Crush Initiators," *Proceedings of ASME International Mechanical Engineering Congress* (2005), 317-326.

47. C.H. Chui, K. Tsai and W.J. Huang, "Crush-Failure Modes of 2D Triaxially Braided Hybrid Composite Tubes," *Composites Science and Technology* 59 (1999), 1713-1723.

48. J.P. Berry, J. Blears, J.D. Grundy, R. Keale, B. Seddeon, R.P. Snowdon and D. Hull, "Energy Absorption Composites Group Report 9," Department of Materials Science and Metallurgy, University of Liverpool (1982).

49. P.H. Thornton, J.J. Harwood and P. Beardmore, "Fiber-Reinforced Plastic Composites for Energy Absorption Purposes," *Composites Science and Technology* 24 (1985), 275-298.

50. P.H. Thornton and A. Jeryan, "Crash Energy Management in Composite Automotive Structures," *International Journal of Impact Engineering* 7, no. 2 (1987), 167-180.

51. N.A. Warrior, T.A. Turner and F. Robitaille, "Effect of Resin Properties and Processing Parameters on Crash Energy Absorbing Composite Structures Made by RTM," *Composites: Part A* 34 (2003), 543-550.

52. E.J. Barbero, *Introduction to Composite Material Design* (Taylor and Francis Group, 1999), 29-32.

53. S. Solaimurugan and R. Velmurugan, "Influence of In-Plane Fibre Orientation on Mode I Interlaminar Fracture Toughness of Stitched Glass / Polyester Composites," *Composites Science and Technology* 68 (2008), 1742-1752.

54. A.P. Mouritz, C. Baini and I. Herszberg, "Mode I Interlaminar Fracture Toughness Properties of Advanced Textile Fibreglass Composites," *Composites: Part A* 30 (1999), 859-870.

55. R.F. Gibson, *Principles of Composite Material Mechanics* (McGraw-Hill, Inc., 1994), 364.

56. J.G. Funk, "The Interlaminar Fracture Toughness of Woven Graphite / Epoxy Composites," *Langley Research Center: NASA* (1989), microfilm.

57. H. Hamada and S. Ramakrishna, "Crushing Mechanism of Carbon Fibre / PEEK Composite Tubes," *Composites* 26 (1995), 749-755.

58. H. Hamada, J.C Coppola, D. Hull, Z. Maekawa and H. Sato, "Comparison of Energy Absorption of Carbon / Epoxy and Carbon / PEEK Composite Tubes," *Composites* 23, no. 4 (1992), 245-252.

59. N.A. Warrior, T.A. Turner, F. Robitaille and C.D. Rudd, "The Effect of Interlaminar Toughening Strategies on the Energy Absorption of Composite Tubes," *Composites: Part A* 35 (2004), 431-437.

60. D. Hull, "Axial Crushing of Fibre Reinforced Composite Tubes," *Structural Crashworthiness* (1983), N. Jones and T. Weirzbicki (eds), 118-135

61. M. Okano, A. Nakai and H. Hamada, "Axial Crushing Performance of Braided Composite Tubes," *International Journal of Crashworthiness* 10, no. 3 (2005), 287-294.

62. N.L. Johnson, A.L. Browne, P.J. Watling and D.G. Peterson, "Parameter effects on the dynamic crush performance of braided 'hourglass' cross section composite tubes," *Proceedings of the 9th Annual ASM/ESD Advanced Composites Conference* (1993), 403–420.

63. G.L. Farley, "The Effects of Crushing Speed on the Energy Absorption Capability of Composite Tubes," *Journal of Composite Materials* 25 (1991), 1314-1329.

64. H. Hamada and S. Ramakrishna, "Effect of Fiber Orientation of the Energy Absorption Capability of Carbon Fiber / PEEK Composite Tubes," *Journal of Composite Materials* 30, no. 8 (1996), 947-963.

65. J. Berry and D. Hull, "Effect of Speed on Progressive Crushing of Epoxy Glass Cloth Tubes," *3rd Conference on Mechanical Properties at High Rates of Strain* (1984), 463-470.

66. A. Brighton, M. Forrest, M. Starbuck, D. Erdman and B. Fox, "Strain Rate Effects on the Energy Absorption of Rapidly Manufactured Composite Tubes," *Journal of Composite Materials* 43, no. 20 (2009), 2183-2200.

67. A.G Mamalis, Y.B. Yuan and G.L. Viegelahn, "Collapse of Thin-Walled Composite Sections Subjected to High Speed Axial Loading," *International Journal of Vehicle Design* 13, no. 5-6, (1992), 564-580.

68. A.G. Mamalis, D.E. Manolakos, G.A. Demosthenous and M.B. Ioannidis, "Axial Collapse of Thin-Walled Fibreglass Composite Tubular Components at Elevated Strain Rates," *Composites Engineering* 4, no. 6 (1994), 653-677.

69. N.A. Warrior, T.A. Turner, E. Cooper and M. Ribeaux, "Effects of Boundary Conditions on the Energy Absorption of Thin-Walled Polymer Composite Tubes Under Axial Crushing," *Thin-Walled Structures* 46 (2008), 905-913.

70. M. Abdel-Haq and G.M. Newez, "Role of Failure Modes on Energy Absorption in Unidirectional PMC Tubes," *Journal of Composite Materials* 35, no. 11 (2001), 941-953.

71. P. Snowdon and D. Hull, "Energy Absorption of SMC Under Crash Conditions", *Proc. Fiber Reinforced Composites Conference* (1984), Plastics and Rubber Institute, 5.1-5.10.

72. G.L. Farley, "Effect of Specimen Geometry on the Energy Absorption Capability of Composite Materials," *Journal of Composite Materials* 20 (1986), 390-400.

73. H. Hamada and S. Ramakrishna, "Scaling Effects in the Energy Absorption of Carbon-Fiber / PEEK Composite Tubes," *Composites Science and Technology* 55 (1995), 211-221.

74. A.M. Elgalai, A.M.S. Hamouda, E. Mahdi and B.S. Sahari, "Energy Absorption Capabilities of Woven Roving Glass / Epoxy Composite Tubes: Effect of Tube Length," *Strength, Fracture and Complexity* 3 (2005), 15-24.

75. J.D. Melo, A.L.S. Silva, J. Edward and N. Villena, "The Effect of Processing Conditions on the Energy Absorption Capability of Composite Tubes," *Composite Structures* 82 (2008), 622-628.

76. Y. Yang, A. Nakai, T. Uozumi and H. Hamada, "Energy Absorption Capability of 3D Braided-Textile Composite Tubes With Rectangular Cross Sections," *Key Engineering Materials* 334-335 (2007), 334-335.

77. P. Feraboli, B. Wade, F. Deleo and M. Rassaian, "Crush Energy Absorption of Composite Channel Section Specimens," *Composites: Part A* 40 (2009), 1248-1256.

78. D.G. Pafitis and D. Hull, "Design of Fiber Composite Conical Components for Energy Absorbing Structures," *SAMPE Journal* 27 (1991), 29-34.

79. G.C. Jacob, J.F. Fellers, S. Simunovic and J.M. Starbuck, "Energy Absorption in Polymer Composites for Automotive Crashworthiness," *Journal of Composite Materials* 36, no. 7 (2002), 813-851.

80. D.M. Garner and D.O. Adams, "Test Methods for Composites Crashworthiness: A Review," *Journal of Advanced Materials* 40, no. 4 (2008), 5-26.

81. P.H. Thornton, "Effect of Trigger Geometry on Energy Absorption in Composite Tubes," *5th International Conference on Composite Materials* (1985), 1183-1199.

82. C.H. Kindervater, "Compression and Crush Energy Absorption Behavior of Composite Laminates," *Advanced Materials and Development for Transport, 8th Symposium* (1985), 289-297.

83. A.G. Mamalis, D.E. Manolakos, M.B. Ioannidis and D.P. Papapostolou, "On the Response of Thin-Walled CFRP Composite Tubular Components Subjected to Static and Dynamic Axial Compressive Loading: Experimental," *Composite Structures* 69 (2005), 407-420.

84. H. Hamada and S. Ramakrishna, "Impact Performance of Glass Cloth / Epoxy Composite Tubes With Different Surface Treatments," *Composite Interfaces* 4, no. 1 (1996), 35-44.

85. V.M. Karbhari and J.E. Haller, "Rate and Architecture Effects on Progressive Crush of Braided Tubes," *Composite Structures* 43 (1998), 93-108.

86. T.J. Brimhall, "Dynamic Energy Absorption Modes of Braided Carbon / Vinyl Ester Composite Crush Tubes," *6th Annual SPE Automotive Composites Conference* 2 (2006), 696-713.

3 STRAIN RATE AND TRIGGER EFFECTS

3.1 Abstract

An investigation into the effect of cross sectional shape, trigger type, and strain rate is presented for IM7/8552 prepreg tubes. Layups were designed so that failure modes represented the three broad classifications (fragmentation, fiber splaying, and brittle fracture) observed in tube specimens during axial crushing. Each of these layups were tested with circular and square cross sections, bevel and tulip triggers, and at quasi-static and dynamic test speeds. Results showed that circular cross sections were more efficient that square cross sections when comparing similar test variables. Tulip triggers were found to increase energy absorption, although only for certain failure modes and only at quasi-static test speeds. Strain rate effects varied widely across cross sectional shape, layup, and trigger type. The differences in energy absorption values when comparing any of testing variables was attributed to changes in the failure mechanisms that occur during crushing.

3.2 Introduction

Understanding the crashworthiness response of composite materials is essential in allowing them to be integrated into today's vehicles as primary structures. It has been shown that when designed correctly composite structures can absorb more energy per unit mass than metallic structures, which would allow reduction in vehicle weights while

maintaining crashworthiness performance.[1,2] Although much has been learned about the crash response of composite structures there are still many variables that are not well understood.

The current understanding of composite crashworthiness relies heavily on mechanical testing. Data from testing leads to material properties and empirical relations that can then be used for design work and analytical models. Mechanical testing is generally broken into three categories: coupons, elements, and structures. Elements, the focus of this research, are self-supporting test samples that incorporate non-planar sections into their geometry. Examples of elements are tubes, cones, sine webs, and channel sections.

Mechanical testing is carried out on mechanical testing machines, drop towers, and servo hydraulic machines to allow testing over a broad range of speeds. Results are typically reported as the amount of energy absorbed per unit mass (in kJ/kg) and given as Specific Energy Absorption (SEA) or Specific Sustained Crushing Stress (SSCS).

3.2.1 Literature Review

Previous research has shown that the energy absorption of element level test samples relies on testing variables including cross sectional geometry, fiber architecture, stacking sequence, trigger type, and strain rate.[3-5] Some variable effects, such as cross sectional shape, are relatively well understood while others, notably strain rate, lack a consensus in the literature.

When reporting and discussing crashworthiness testing results the failure modes occurring in the specimen are often of interest. Stable, or continuous, failure modes are of

the utmost importance as they allow the highest energy absorption values for any given structure. This is in contrast to unstable failures such as buckling and fracture. Stable failures are further divided into three broadly classified failure modes: fragmentation, fiber splaying, and brittle fracture.[3-5] A summary of failure modes and their characteristics is presented in Table 3.1.

3.2.1.1 Failure Modes

3.2.1.1.1 Fragmentation. Figure 3.1a shows a cross section of a tube wall failing in a typical fragmentation mode. Fragmentation is characterized by short (less than the tube wall thickness) interlaminar, intralaminar, and axial cracks. During crushing, pieces of the tube wall shear off on inclined planes forming ring-like debris. Failure is due to a combination of fiber fracture, matrix fracture, buckling of the fibers, and interlaminar cracks.[3] After a piece shears off, the load is taken up by the remaining tube wall until a critical load is reached, at which point another piece shears off and the process is repeated. This process has been shown to be essentially self stabilizing for certain fiber architectures, meaning that different initial conditions, such as trigger angle, will result in the same failure mode.[6] The primary energy absorbing mechanisms are fiber and matrix fracture.

3.2.1.1.2 Fiber splaying. Figure 3.1b shows a cross section of a tube wall failing in a typical fiber splaying mode. Fiber splaying is characterized by long (greater than the tube wall thickness) interlaminar, intralaminar, and axial cracks. These cracks separate the tube wall into fiber bundles, known as fronds, which bend to the inside or outside of the tube as it is crushed.[7] The majority of the fiber bundles do not fracture as they

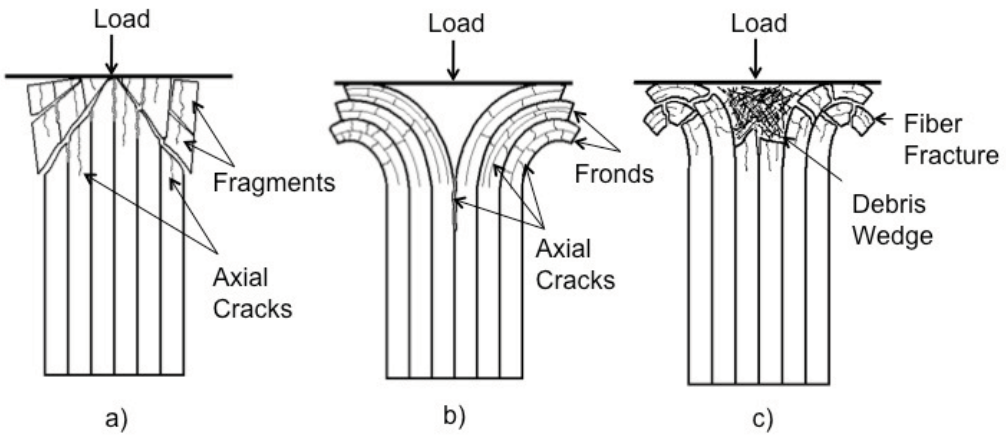

Figure 3.1: Failure modes showing (a) fragmentation, (b) fiber splaying, and (c) brittle fracture.

are bent against the loading surface. Failure is due to crack growth and compression and bending stresses. The primary energy absorbing mechanisms include the energy associated with crack formation, bending of fronds, and various forms of friction such as the fronds against the loading surface and fronds on other fronds as they are bent through different radii of curvatures.[3]

3.2.1.1.3 Brittle fracture. Figure 3.1c shows a cross section of a tube wall failing in a typical brittle fracture mode. Brittle fracture is essentially a combination of fragmentation and fiber splaying with characteristics inherent to both: axial cracks are present and fronds are formed. However, the fronds are bent through a small enough radius that nearly all of them fracture. Near the center of the tube wall, material that is not divided into fronds fails due to compressive stresses and forms an area of crushed material, known as a debris wedge.[7] Energy absorbing mechanisms include contributions from fiber and matrix fracture, crack growth, frond bending, and frictional effects.

3.2.1.2 Cross Sectional Shape

Several researchers have compared the specific energy absorption values of circular and square cross sections. Thornton[2,8] found that square and rectangular cross sections absorbed less energy than circular cross sections. This same trend has been noted by other authors for several fiber architectures.[9-11] Feraboli,[12] using various channel and corner sections, found that elements containing small planar sections had higher SEA values than those with larger plane sections. Kindervater[13] and Bulokbasi et al.[14] reported similar results with angle and channel sections. Differences in energy absorption between circular and square cross sections were attributed to the failure mechanisms that occur in planar and corner (or arced) portions of the tube. Planar sections have been shown to be prone to delamination whereas corner, or arced, sections produce local tearing of the laminate.[12] The additional energy associated with laminate tearing around the perimeter of circular tubes accounts for the increase in SEA when compared to square tubes.

Table 3.1: Failure Mode Summary

	Fragmentation	Fiber Splaying	Brittle Fracture
Characteristics	Short axial cracks. Sections of structure wall are sheared off. No debris wedge present.	Long axial cracks. Fronds are developed but do not fracture. Small debris wedge may be present.	Intermediate length axial cracks. Fronds develop and fracture. Large debris wedge present.
Failure Mechanisms	Fiber and matrix fracture.	Mode I and II fracture.	Mode I and II fracture. Fiber and matrix fracture.
Energy Absorption Mechanisms	Fiber and matrix fracture.	Friction, crack growth, frond bending.	Friction, fiber and matrix fracture, crack growth.

3.2.1.3 Trigger Type

Triggers are geometric modifications made to one end of a test sample that promotes failure by increasing local stresses.[2] Triggers allow the sample to crush stably at loads lower than the ultimate compressive load. Two of the most common trigger types are bevel triggers and tulip triggers, shown in Figure 3.2. Angling the tube wall relative to a line going through the wall thickness creates a bevel trigger. Angling the tube wall relative to a line going around the perimeter creates a tulip trigger.

Bevel triggers are commonly used due to their ease of manufacturing. However, tulip triggers have been investigated by several authors for square cross sections. Tulip triggers have been shown to increase SEA values up to 20% when compared to similar tubes using bevel triggers.[15-17]

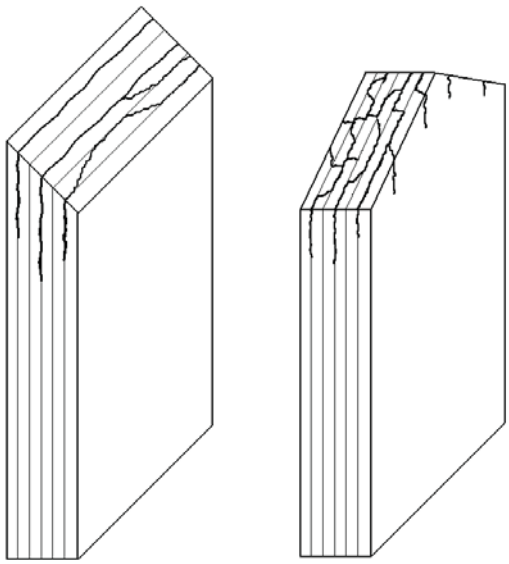

Figure 3.2: Bevel (left) and tulip trigger (right) showing introduced crack orientation.

It has been noted that a key difference between bevel and tulip triggers is the length and orientation of the axial cracks that are introduced during crushing.[6,15,16] Both triggers tend to promote cracks that are parallel to the apex of the trigger in the axial direction.[17] The bevel trigger promotes cracks in line with the relatively weak lamina interfaces and allows delamination. The tulip trigger, in contrast, promotes cracks that are normal to the lamina interfaces and allows different failure mechanisms, including material fracture, to occur. It is this difference that provides tulip triggers with higher SEA values than bevel triggers for similar tubes. It should be noted that the research referenced involves testing at quasi-static test speeds only.

3.2.1.4 Strain Rate

Currently, there is no consensus in the literature on the effect of strain rate on energy absorption. Different researchers have reported no changes, increases, and decreases in SEA values as test speeds increase from quasi static to dynamic rates. Several review articles have compiled testing data for different fiber and matrix types, architectures, and strain rates.[3-5,18] Strain rate testing results for unidirectional carbon fiber/epoxy prepreg are shown in Table 3.2, where the failure modes listed are those described in Section 1.1.

A common theory is that energy absorption is a function of strain rate if the failure mechanisms occurring during crushing are also a function of strain rate.[22] It is therefore reasonable that each failure mode described previously in Section 1.1, with their associated failure mechanisms, may behave differently when comparing quasi-static and dynamic test speeds. It has been observed that failure modes have the potential to change

Table 3.2: Strain Rate Testing Summary

Author(s)	Fiber Material	Matrix Material	Layup	Rates Tested	Failure Modes	Results
Farley [19]	Carbon	Epoxy	[0/±θ], [±45]	$1.3x10^{-7}$ – 7 m/s	Brittle Fracture (constant)	Rate independent
Farley [20]	Carbon	Epoxy	[0/±θ]	0.01 – 12 m/s	Brittle Fracture (constant)	Rate independent
Farley [20]	Carbon	Epoxy	[±θ]	0.01 – 12 m/s	Brittle Fracture / Fragmentation (constant)	Increase up to 35%
Schmueser Wickliffe [21]	Carbon	Epoxy	[0/±45]	$1.7x10^{-4}$ – 5 m/s	Fiber Splaying / Brittle Fracture (constant)	Decrease up to 30%

with strain rate, making broad statements about strain rate response nearly impossible for all material types and geometries.[23-27]

3.3 Materials and Methods

3.3.1 Tube Manufacturing

In order to investigate strain rate and triggering effects for all failure modes, laminate stacking sequences were designed that would produce fragmentation ([F]), brittle fracture ([B]), and fiber splaying ([S]) failure modes. Stacking sequences from the literature and their observed failure modes were used as a starting point. Following initial testing, crushed test samples were potted in clear polyester casting resin and sectioned, polished, and photographed. Several iterations were required to identify laminates that produced the desired failure modes. The final laminate stacking sequences and photomicrographs of their observed failure modes are shown in Table 3.3. Note that these failure modes were only observed for circular tubes with bevel triggers tested at a quasi-

static rate. Differences in failure modes for each shape, trigger, and test speed were expected.

Circular and square tubes were created using a roll wrapping method. 6061-T6 aluminum mandrels 275 mm long were cut from 50 mm round aluminum and 50 mm square aluminum extrusions. Mandrels were tapered 0.25° to facilitate easy removal of the tubes. This small angle of taper should not affect the results of tube samples when compared to perfectly prismatic tubes based on results from Ochelski and Gotowicki.[28] A 6.4 mm corner radius was milled onto the square mandrels. The mandrels were sanded with 800 grit sandpaper and prepped with PTFE mold release spray.

Plies were cut from 305 mm wide Hexcel IM7/8552 prepreg 0.131 mm thick (cured ply thickness). The cut plies were 229 mm long and wide enough to allow 2.5 mm of overlap for the outermost ply. A 5 g/m^2 carbon fiber veil was used as the innermost

Table 3.3: Stacking Sequences and Photomicrographs

	Fragmentation [F]	Brittle Fracture [B]	Fiber Splaying [S]
Layup	$[(90_2/\pm60)_2]_s$	$[90_2/\pm45_2/0_2]_s$	$[90/(\pm30/0)_2/0]_s$
Photomicrograph	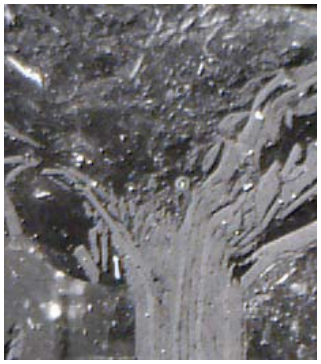		

layer to allow the mandrels to expand and contract without distorting the first prepreg layer. Mold tactifier was used to facilitate easy attachment of the first ply. Additional layers were placed in order, one at a time, and situated so that the seams created by each layer were spaced evenly around the perimeter of the tube. Each tube consisted of 16 plies.

Tube compaction was provided by polyester shrink tape. For circular mandrels 12 mm shrink tape was laid on with 3.5 N of tension with an overlap distance of 3.2 mm. For square tubes 12 mm shrink tape was laid on with 1.5 N of tension and 3.2 mm of overlap to provide compaction on the corners. To provide compaction on the planar section the method described by Schultz[29] was used. Polyester shrink tape that was 32 mm wide was laid over the aluminum T-bars with 15 N of tension and 6.4 mm of overlap. Silicon rubber was placed against the T-bars to allow even pressure distribution. A square tube wrapped and ready for cure is shown in Figure 3.3.

Tubes were cured using a modified Hexcel cure cycle for IM7/8552 prepreg. The oven temperature was increased from room temperature to a soak temperature of 107 C. The soak time at 107 C was increased from the recommended 60 minutes to 80 minutes to allow the relatively thick mandrels to heat to a near constant temperature. The temperature was then increased to 160 C for a time of 120 minutes to allow full cure.

Post-cure measurements determined that the average wall thickness of circular tubes was 2.21 mm (*SD* = 0.18 mm) compared to the expected thickness of 2.24 mm. The planar sections of the square tubes averaged 2.16 mm (*SD* = 0.085 mm) thick and the corners averaged 2.03 mm (*SD* = 0.08 mm) thick. The difference in thickness between corner and planar sections was 12%. This difference includes the thickness increases

Figure 3.3: Square tube shrink wrapped and ready for curing.

for the overlap of plies. The average density of the tubes was 1.61 g/cm^3 (*SD* = 0.04 g/cm^3).

Following tube manufacturing, 12 mm was trimmed from each end and the tubes were cut to the desired lengths for quasi-static or dynamic testing. Triggers were introduced to the smaller of the two ends of the tube (resulting from the taper) in two separate methods. Bevel triggers were ground at 45° into the ends of the tube using an alignment jig and a sanding disk with 120 grit abrasive. Tulip triggers were cut into the ends of the tube at 20° using a diamond cutting disk and an alignment jig to ensure the cut was square to the tube wall.

3.3.2 Tube Testing

Each of the three layups ([F], [B], and [S]) were tested using circular and square tubes, bevel and tulip triggers, and at quasi-static and dynamic rates. Three tubes were tested for each condition.

3.3.2.1 Quasi-Static Testing

Quasi-static tube testing was performed at 4.23 x 10^{-4} m/s (25.4 mm/min) using an electromechanical test machine. Test samples were 100 mm long and were crushed for 50 mm during testing. Load and displacement data were collected for each sample. Tubes were crushed against AISI 1020 10 ga. cold rolled steel sheet, with a new piece used for each test to provide a common crushing surface. The average hardness of the testing surface was measured at 67.5 HRB. Alignment was ensured by a two-post press die set.

3.3.2.2 Dynamic Testing

Dynamic testing was performed at Oak Ridge National Laboratory using the Test Machine for Automotive Crashworthiness (TMAC). TMAC is an open-loop servo-hydraulic machine capable of constant velocity testing at speeds of up to 8 m/s. Tube test samples were 200 mm long and crushed for a distance of 100 mm at 6 m/s. Load and displacement data, along with high speed video, were collected for each test. Only the first 50 mm of data were used for analysis, as the final 50 mm include the hydraulic ram slowing to a rest. Samples were not supported or aligned during loading. Test samples were crushed against 1020 10 ga. cold rolled steel sheet with a new piece for each test.

3.4 Results

3.4.1 Data Interpretation

Tables 3.4 and 3.5 contain a summary of testing for quasi static and dynamic test speeds, respectively. The average and standard deviation for each test group is given.

The Specific Sustained Crushing Stress (SSCS) method was used to interpret the load curves. SSCS is the value of average stress during stable crushing divided by the density of the material,[19] or

$$SSCS = \frac{\overline{\sigma}}{\rho}. \tag{3.1}$$

Stable failure was determined to begin at the local minimum following the peak load of the initial slope of the load curve. A curve showing points of interest and a sample calculation is shown in Figure 3.4.

A four-way ANOVA was performed examining layup, cross sectional shape, trigger type, and test speed effects on SSCS values. Significant differences in SSCS

Table 3.4: Summary of Quasi-Static Testing Results

Fiber Layup	SSCS Average and (STDV) in kJ/kg			
	Circular Tubes		Square Tubes	
	Bevel Trigger	Tulip Trigger	Bevel Trigger	Tulip Trigger
[F]	79.5 (6.5)	70.3 (2.2)	48.8 (2.8)	43.2 (4.8)
[B]	82.8 (5.0)	93.7 (10.5)	46.8 (6.6)	65.8 (8.5)
[S]	99.4 (6.3)	124.0 (5.9)	52.4 (3.2)	100.6 (3.7)

Table 3.5: Summary of Dynamic Testing Results

Fiber Layup	SSCS Average and (STDV) in kJ/kg			
	Circular Tubes		Square Tubes	
	Bevel Trigger	Tulip Trigger	Bevel Trigger	Tulip Trigger
[F]	46.7 (2.6)	48.2 (0.7)	36.3 (3.7)	35.6 (2.7)
[B]	68.6 (3.0)	69.3 (4.1)	47.8 (2.5)	54.8 (1.0)
[S]	95.3 (2.0)	102.1 (11.3)	71.2 (7.6)	75.9 (5.4)

values were seen for all of the main variable effects ($p < .0001$). In addition, significant differences ($p < .0001$) in SSCS values were observed due to interactions between several of these variables. Significant interactions occurred for trigger type and layup, cross sectional shape and test speed, and trigger type and test speed. These results are presented and discussed in the following sections.

3.4.2 Specimen Geometry Effects

Results for circular and square cross sections can be seen in Tables 3.4 and 3.5. Similar to results in the literature[8-11] circular cross sections were found to produce higher average SSCS values than square cross sections for all layups, triggers, and test speeds.

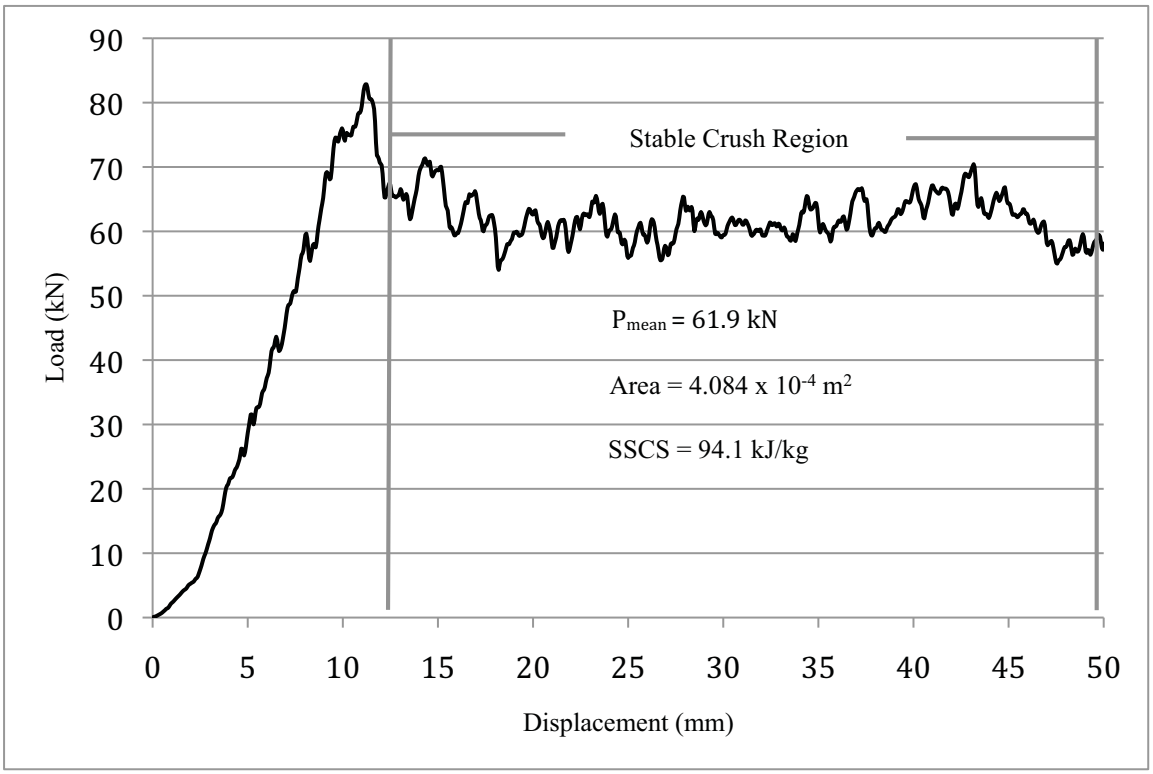

Figure 3.4: Sample load curve showing stable crush region and sample calculation.

The increase in average SSCS value for circular tubes compared to square tubes with similar testing variables ranged from 20% to 90%.

3.4.3 Trigger Effects

Figures 3.5 and 3.6 show SSCS values for circular and square tubes when tested with bevel and tulip triggers quasi-statically. For [F] layups, tulip triggers offered no apparent increase in SSCS values when compared to bevel triggers. For [B] layups, tulip triggered tubes had increased average SSCS values, but the increase was only statistically significant (p = .036) for the square cross section. The [S] layup showed increases in average SSCS values for tulip-triggered tubes of approximately 25% for circular cross sections and 92% for square cross sections.

Changes in SSCS values between bevel and tulip triggered tubes when tested dynamically can be seen comparing Tables 3.4 and 3.5. SSCS increases for tulip triggered were much less than those observed during quasi-static testing and ranged from roughly 0% to 15%.

3.4.4 Strain Rate Effects

Figures 3.7 and 3.8 show circular and square tubes with bevel triggers tested quasi-statically (4.23×10^{-4} m/s) and dynamically (6 m/s). A comparison of tulip triggers

can be made by comparing Tables 3.4 and 3.5. These results are more difficult to interpret than those presented in the previous section, but several observations can be made. For both shapes and trigger types a decrease occurred in average SSCS values for [F] layups when comparing quasi-static to dynamic test speeds. Decreases in average

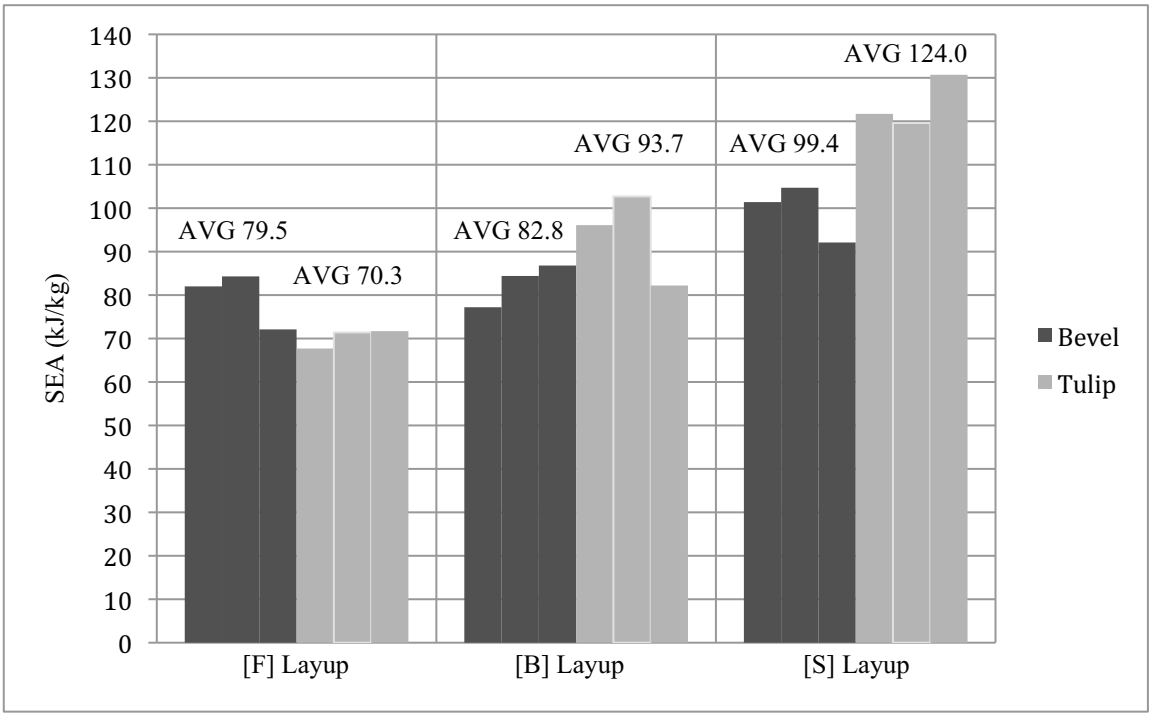

Figure 3.5: SSCS comparison of circular tubes with bevel and tulip triggers tested quasi-statically.

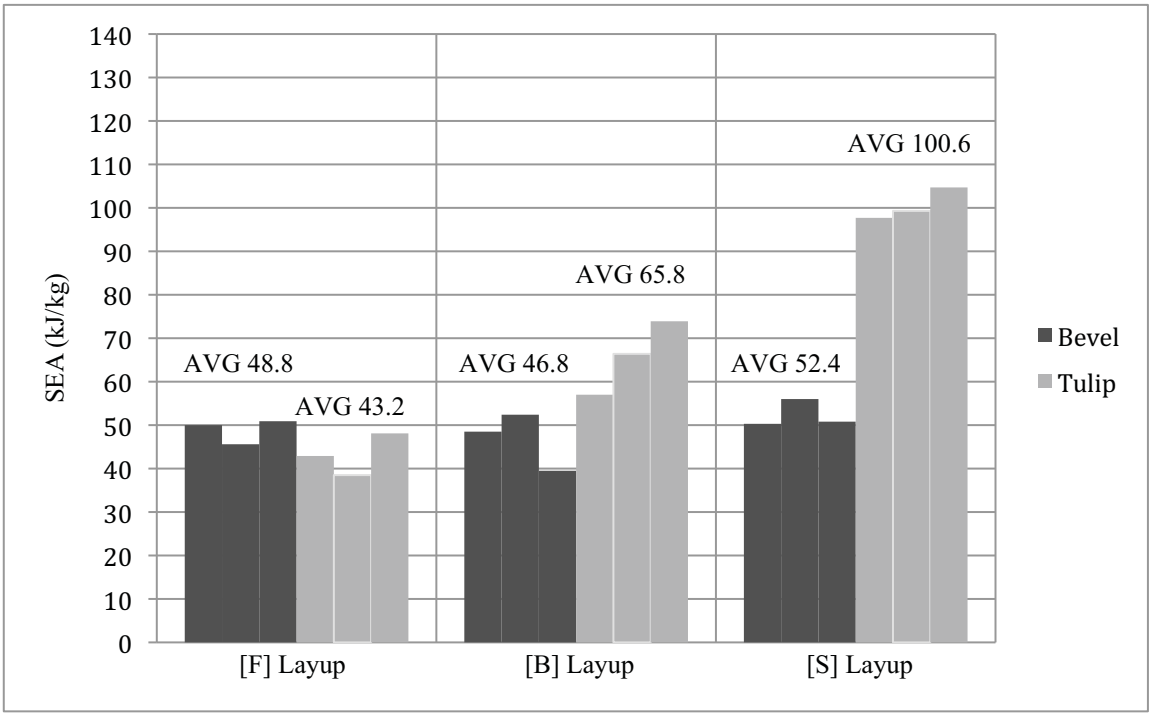

Figure 3.6: SSCS comparison of square tubes with bevel and tulip triggers tested quasi-statically.

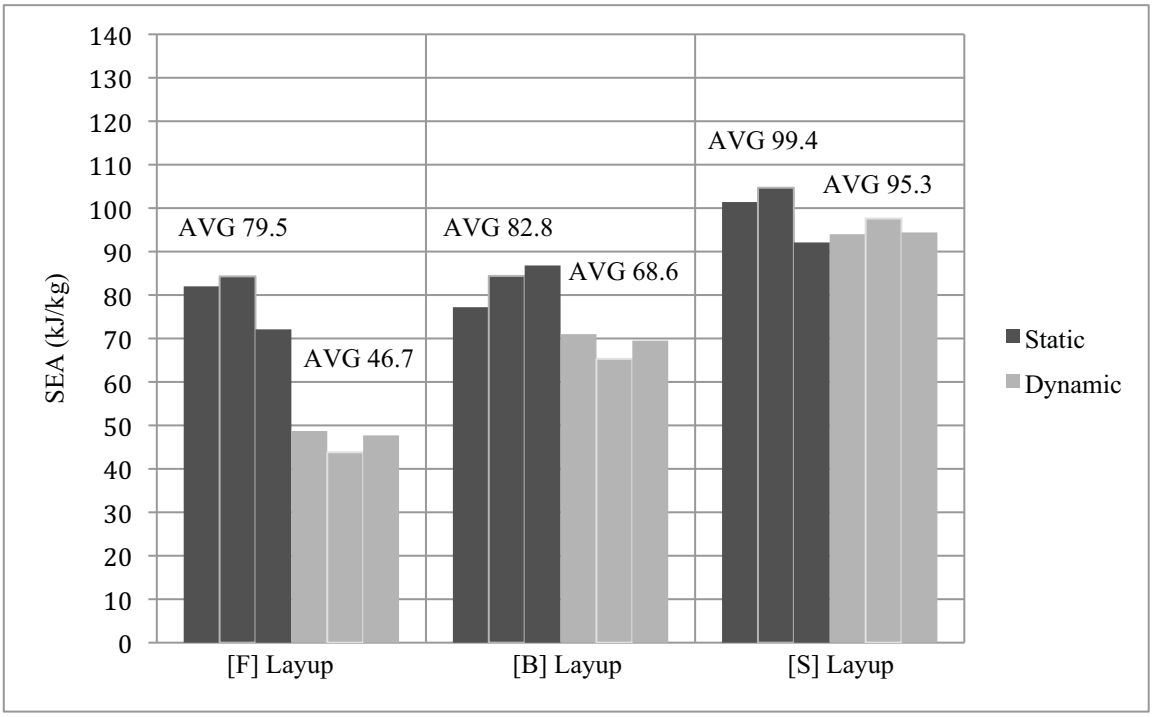

Figure 3.7: SSCS comparison of circular tubes with bevel trigger tested quasi-statically (4.23×10^{-4} m/s) and dynamically (6 m/s).

SSCS value varied from approximately 20% to 40%.

For circular [B] tubes with both trigger types there was a decrease in average SSCS values for dynamic test speeds, ranging from 17% to 26%. For circular [S] tubes there was little change in average SSCS value for bevel triggers but a decrease of 18% for tulip triggers.

For the square tubes, the changes in SSCS values from quasi-static to dynamic test speeds were less consistent. For the [B] layup there was no change in average SSCS value for dynamic test speeds when using the bevel trigger. However, a 17% drop in average SSCS value was observed when using a tulip trigger. For the [S] layup there was a 36% increase in the average SSCS value for the bevel trigger and a 25% decrease for the tulip trigger.

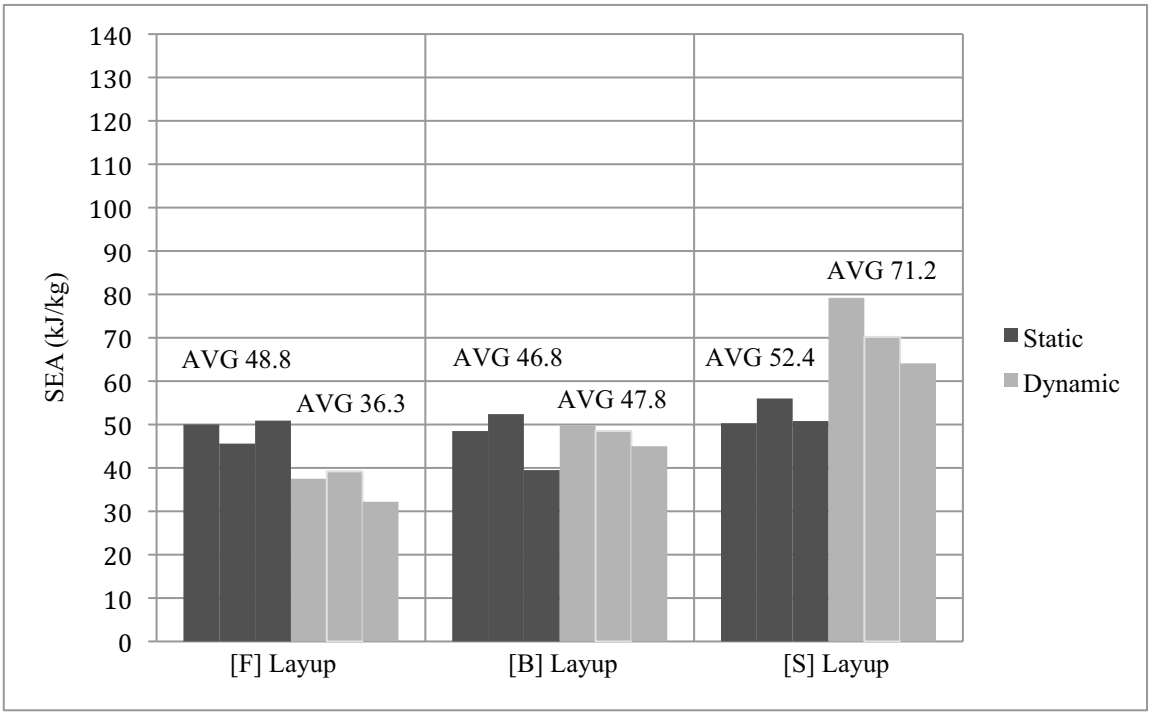

Figure 3.8: SSCS comparison of square tubes with bevel trigger tested quasi-statically (4.23×10^{-4} m/s) and dynamically (6 m/s).

3.5 Discussion

3.5.1 Specimen Geometry

The literature review suggests that circular cross sections absorb more energy per unit mass than square cross sections for similar test variables.[8-11,16] The difference in energy absorption is attributed to the different failure modes that occur for corner, or arced sections, compared to a planar section. To illustrate this Figure 3.9 shows post-crush failure characteristics of circular and square [B] layup tubes with tulip triggers tested at 4.23×10^{-4} m/s. It can be seen that the planar sections of the square tube have delaminated with laminate tearing occurring at the four corners. The circular tube contains many laminate tears around the perimeter with little delamination. The relatively high energy absorption associated with laminate tearing and a small amount of

Figure 3.9: Post-crush characteristics of circular and square [B] tubes with tulip triggers from quasi-static testing.

accompanied delamination (a relatively low energy absorption mechanism) provides the circular cross sections with higher SSCS values.

3.5.2 Trigger Type

The trigger effects on the layups tested for this investigation tested were highly layup and rate dependent. For quasi-static test speeds, the trigger effects were based on the length and orientation of axial cracks that form from each trigger. For [F] tubes, which have very short axial cracks, the cracks introduced by either trigger type were contained within the material that is sheared off during fragmentation. Thus, the tulip trigger offered no advantage to the bevel trigger.

For [B] layups the length and orientation of axial cracks formed during crushing affected the type of failure mechanisms that occurred. It appears that these shifts in failure mechanisms were slight for the circular cross sections and more substantial for the square cross sections, explaining the noticeable increases in SSCS for the square [B] tulip triggered tubes.

For the [S] layup, which contains the longest axial cracks, the changes in failure mechanisms caused by the tulip trigger provide a large increase in SSCS values. This was particularly effective for the square cross section, which benefited from cracks oriented normal to the interlaminar boundaries to help limit delamination. Changes in failure mechanisms can be seen in Figure 3.10. Note the delamination occurring in the bevel triggered tube and the increased fiber and matrix fracture occurring in the tulip triggered tube.

Trigger type had far less effect on the SSCS of tubes tested at dynamic test speed, as discussed in the following section.

3.5.3 Strain Rate

Results from the literature for strain rate testing of carbon fiber/epoxy prepreg tubes (shown previously in Table 3.2) do not indicate drastic changes in failure modes as strain rate increases. The research referenced, however, used different stacking sequences from

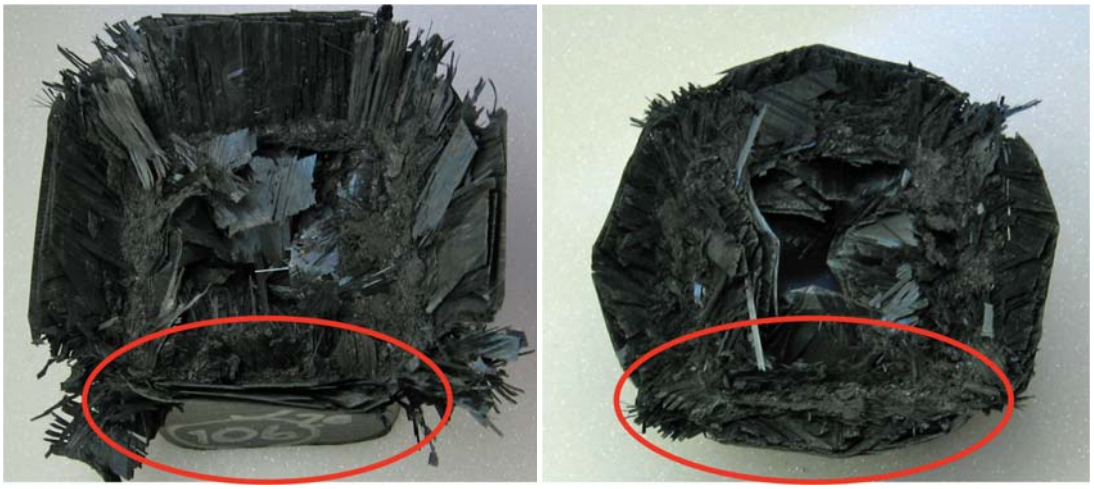

Figure 3.10: Postcrush square [S] tubes with bevel (left) and tulip (right) triggers showing changes in failure mechanisms.

those in this study and relied on macroscopic observations only. Differences between the literature and this investigation are expected.

Several of the trends observed when comparing the SSCS of the two different test speeds can be attributed to the change in failure mode. Photomicrographs from dynamic testing are shown in Table 3.6. Comparisons of Table 3.3 and Table 3.6 will allow a visual reference of the results described in this section.

The consistent and significant drop in SSCS for the [F] tubes for both shapes and trigger types can be explained by a shift to a brittle fracture type failure mode at 6 m/s compared to the fragmentation type of failure experienced at 4.2 x 10^{-4} m/s. For the failure at 6 m/s there would be less energy absorption due to fiber and matrix fracture and more due to crack growth, frond bending, and friction. However, the axial stiffness and strength of plies in the 60° and 90° orientations are much less than those seen in the 0°, 30°, and 45° plies in the [B] or [S] laminates, and therefore would absorb comparatively

Table 3.6: Dynamic Photomicrographs of [F], [B], and [S] Layups

	Fragmentation [F]	Brittle Fracture [B]	Fiber Splaying [S]
Layup	$[(90_2/\pm60)_2]_s$	$[90_2/\pm45_2/0_2]_s$	$[90/(\pm30/0)_2/0]_s$
Micrograph			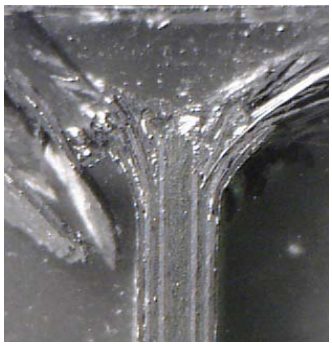

less energy from these mechanisms. The results would suggest that the energy from crack growth, frond bending, and friction are not enough to overcome the loss of energy from fiber and matrix fracture.

The failure mode shifts for the [F] tubes are likely the result of strain rate-induced increases of the compression and interlaminar shear strength of the material and a transition to brittle behavior of the matrix at high test speeds. Transverse compression results for IM7/8552 show an increase in ultimate strength of 40% for 90 and ±60 degree plies for high strain rates.[30] A similar increase was seen for in plane shear strength. Therefore, at dynamic test speeds the tube walls of the [F] layup are able to resist higher compressive and shear strengths. This strength increase could potentially allow crack growth before shear failure of the tube wall, leading to a brittle fracture type failure. It is also suspected that the matrix behaves in a brittle manner and is prone to pulverization at dynamic test speeds. Although matrix pulverization was not observed directly for the [F] layup it can be seen in the [B] and [S] layups in their post crush photomicrographs.

The [B] tubes experienced some failure mode changes during dynamic testing. Increases in fiber fracture and decreases in frond formation and axial cracking were observed. The transition of the matrix to brittle behavior at high strain rates is likely responsible for theses changes. Dynamic SSCS values for [B] tubes were seen to be generally less than static values, varying from approximately equal to 30% less.

The effect of dynamic loading on [S] tubes was dependent on tube cross section and trigger type, as seen in Tables 3.4 and 3.5. Circular tubes experienced lower SSCS values at high strain rates. As shown in Table 3.6, the prominent fronds and long central crack are no longer present in circular tubes at 6 m/s. The brittle behavior of the matrix at

high strain rates, similar to that seen in the [B] tubes, is though to be the cause. Changes in SSCS values are due to the changes in failure mechanisms and their related energy absorption. That is, energy absorbed by crack growth and friction is replaced by fiber and matrix fracture.

The effect of the trigger type on SSCS values during dynamic test speeds for [B] and [S] tubes does not appear to have a pattern when compared to the quasi static test speeds. It can be seen from Table 3.5, however, that the tubes tended to have similar SSCS values for dynamic testing regardless of trigger type. This result is believed to be due to the brittle behavior of the matrix at high test speeds. During quasi static testing substantial frond formation and axial cracking was observed (Table 3.3, [B] and [S] layups). During dynamic testing, however, these failure mechanisms were minimal (Table 3.6, [B] and [S] layups). This behavior occurs because the matrix cannot undergo appreciable strain at dynamic test speeds. Any fronds that are formed fractures off as they are deflected. Therefore, regardless of trigger type similar failure modes and SSCS values occur at dynamic test speeds for the [B] and [S] laminates. A comparison of [S] tubes (the failure most affected by trigger type at the quasi static speed) with bevel and tulip triggers tested at 6 m/s is shown in Figure 3.11.

3.6 Conclusions

The findings of this investigation are as follows:

- Circular cross sections absorbed significantly more energy per unit mass than square cross sections when using identical testing variables (layup, trigger, test rate).

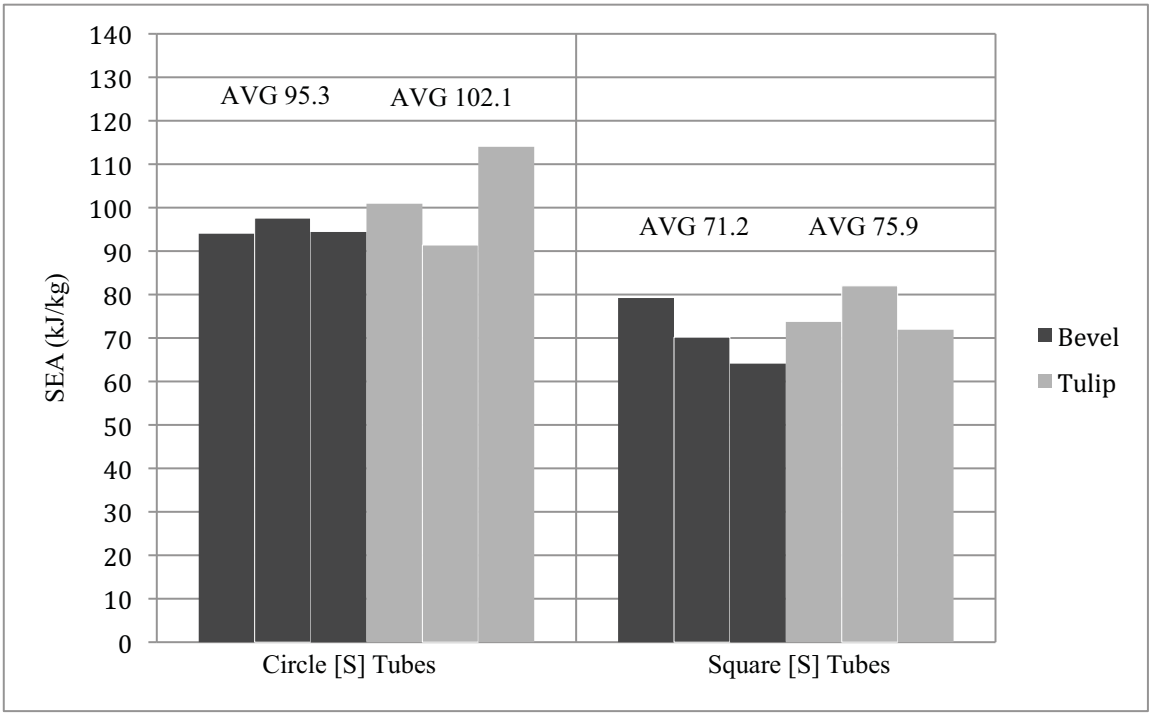

Figure 3.11: SSCS comparison of [S] layup tubes with bevel and tulip triggers tested at 6 m/s.

- Tulip triggers, when compared to bevel triggers, only increased energy absorption for layups that fail in brittle fracture or fiber splaying type failure modes at quasi static test speeds. At dynamic test speeds the response of the matrix prevented substantial frond formation and axial cracking, which resulted in similar SSCS values regardless of trigger type.
- Changes in energy absorption for all variables (geometry, trigger, and test rate) are due to changes in failure mechanisms that occur during crushing and their contribution to the total energy absorbed

These finding reinforce the need for mechanical testing as an important initial step when evaluating composites for crashworthiness applications. Differences in energy absorption values due to variables such as layup, trigger type, and strain rate are

significant and not easily predicted. Continuing investigation into the effect of testing parameters using different material systems will be essential to incorporate composites safely into primary vehicle structures.

3.7 References

1. C.L. Magee and P.H. Thornton, "Design Considerations in Energy Absorption by Structural Collapse," *SAE Prepr*, n 780434, 1978, February 27 – March 3.

2. P.H. Thornton, "Energy Absorption in Composite Structures," *Journal of Composite Materials* 13 (1979), 247-62.

3. S. Ramakrishna and H. Hamada, "Energy Absorption Characteristics of Crash Worthy Structural Composite Materials," *Key Engineering Materials* 141-143 (1998), 585-620.

4. J.J. Carruthers, A.P. Kettle and A.M. Robinson, "Energy Absorption Capability and Crashworthiness of Composite Material Structures: A Review," *Applied Mechanics Review* 51, no. 10 (1998), 635-649.

5. G.C. Jacob, J.F. Fellers, S. Simunovic and J.M. Starbuck, "Energy Absorption in Polymer Composites for Automotive Crashworthiness," *Journal of Composite Materials* 36, no. 7 (2002), 813-851.

6. I. Sigalas, M. Kumosa and D. Hull, "Trigger Mechanisms in Energy Absorbing Glass Cloth/Epoxy Tubes," *Composites Science and Technology* 40 (1991), 265-287.

7. G.L. Farley and R.M. Jones, "Crushing Characteristics of Continuous Fiber-Reinforced Composite Tubes," *Journal of Composite Materials* 26 (1992) 37-50.

8. P.H. Thornton and P.J. Edwards, "Energy Absorption in Composite Materials," *Journal of Composite Materials* 16 (1982), 521-545.

9. M.R. Schultz and M.W. Hyer, "Static Energy Absorption Capability of Graphite-Epoxy Tubes," *Journal of Composite Materials* 35, no. 19 (2001), 1747-1761.

10. N.A. Warrior, T.A. Turner, E. Cooper and M. Ribeaux, "Effects of Boundary Conditions on the Energy Absorption of Thin-Walled Polymer Composite Tubes Under Axial Crushing," *Thin-Walled Structures* 46 (2008), 905-913.

11. J.D. Melo, A.L.S. Silva, J. Edward and N. Villena, "The Effect of Processing Conditions on the Energy Absorption Capability of Composite Tubes," *Composite Structures* 82 (2008), 622-628.

12. P. Feraboli, B. Wade, F. Deleo and M. Rassaian, "Crush Energy Absorption of Composite Channel Section Specimens," *Composites: Part A* 40 (2009), 1248-1256.

13. C.M. Kindervater, "Crash Impact Behavior and Energy Absorbing Capability of Composite Structural Elements," *30th International National SAMPE Symposium* (1985), March 19-21.

14. A.O. Bolukbasi and D.H. Laananen, "Energy Absorption in Composite Stiffeners," *Composites* 26 (1995), 291-301.

15. M.J. Czaplicki, R.E. Robertson and P.H. Thornton, "Comparison of Bevel Tulip Triggered Pultruded Tubes For Energy Absorption," *Composites Science and Technology* 40 (1990), 31-46.

16. M.J. Czaplicki, P.H. Thornton and R.E. Robertson, "Collapse Triggering of Polymer Composite Energy Absorbing Structures," *How to Apply Advanced Composites Technology* (American Society for Metals, 1988), 39-46.

17. P.H. Thornton, "Effect of Trigger Geometry on Energy Absorption in Composite Tubes," *5th International Conference on Composite Materials* (1985), 1183-1199.

18. M.A. Courteau and D.O. Adams, "Composite Tube Testing For Crashworthiness Applications: A Review," *Journal of Advanced Materials* 43, no. 2 (2011), 13-34.

19. G.L. Farley, "Energy Absorption of Composite Materials," *Journal of Composite Materials* 17 (1983), 267-279.

20. G.L. Farley, "The Effects of Crushing Speed on the Energy Absorption Capability of Composite Tubes," *Journal of Composite Materials* 25 (1991), 1314-1329.

21. D.W. Schmueser and L.E. Wickliffe, "Impact Energy Absorption of Continuous Fiber Composite Tubes," *Journal of Engineering Materials Technology* 109 (1987), 72-77.

22. A.G. Mamalis, M. Robinson, D.E. Manolakos, G.A. Demosthenous, M.B. Ioannidis and J. Carruthers, "Crashworthy Capability of Composite Material Structures," *Composite Structures* 37 (1997), 109-134.

23. J. Berry and D. Hull, "Effect of Speed on Progressive Crushing of Epoxy Glass Cloth Tubes," *3rd Conference on Mechanical Properties at High Rates of Strain* (1984), 463-470.

24. P.H. Thornton, "The Crush Behavior of Pultruded Tubes at High Strain Rates," *Journal of Composite Materials* 24 (1990), 594-615.

25. H. Hamada and S. Ramakrishna, "Impact Performance of Glass Cloth / Epoxy Composite Tubes With Different Surface Treatments," *Composite Interfaces* 4, no. 1 (1996), 35-44.

26. H. Hamada and S. Ramakrishna, "Comparison of Static and Impact Energy Absorption of Carbon Fiber / PEEK Composite Tubes," *Composite Materials: Testing and Design 12th ed* (1994), R.B. Deo and C.R. Saff (eds), 182-198.

27. V.M. Karbhari and J.E. Haller, "Rate and Architecture Effects on Progressive Crush of Braided Tubes," *Composite Structures* 43 (1998), 93-108.

28. S. Ochelski and P. Gotowicki, "Experimental Assessment of Energy Absorption Capability of Carbon-Epoxy and Glass-Epoxy Composites," *Composite Structures* 87 (2009), 215-224.

29. M.R. Schultz, "Energy Absorption Capacity of Graphite-Epoxy Composite Tubes," M.S. Thesis, Dept. of Engineering Mechanics, Virginia Polytechnic Institute and State University (1998).

30. H. Koerber, J. Xavier and P.P. Camanho, "High Strain Rate Characterization of Unidirectional Carbon-Epoxy IM7-8552 in Transverse Compression and In-plane Shear Using Digital Image Correlation," *Mechanics of Materials* 42 (2010), 1004-1019.

APPENDIX A

CRASHWORTHINESS DATA ANALYSIS

A.1 Characterizing Energy Absorption

There are two common methods of characterizing the energy absorption performance of a material. They are known as Specific Energy Absorption (SEA) and Specific Sustained Crushing Stress (SSCS). Both require the resulting load versus displacement curve from a crush test.

A.1.1 Specific Energy Absorption (SEA)

SEA is the total energy absorbed by a test sample divided by the mass that sustains damage during crushing. It has several advantages and disadvantages over the SSCS method of measurement.

Advantages

- It does not rely on the shape of the load curve
    - Test samples experiencing increasing, decreasing, or erratic loads can be easily accommodated
- It is a true measure of the total energy absorbed by the specimen
    - The SEA method takes the entire load curve into account
- It can be used for specimens that fail in an unstable manner

- There does not need to be any amount of stable crush to use the SEA method

Disadvantages

- It require additional calculations

The total energy under the curve (W) is found by the trapezoidal numerical integration method, which allows for simple calculations with any spreadsheet program. *n* is the number of points between *a* and *b*.

$$\int_a^b f(x)dx \approx \sum_1^n (x(n+1) - x(n))\left(\frac{f(n) + f(n+1)}{2}\right) \qquad \text{(A.1)}$$

The total energy (W) is divided by the cross sectional area of the test sample (A), density of the material (ρ), and total crushed length of the specimen (δ). It is assumed that the total crushed length is equal to the displacement of the crosshead, which has been shown to be approximately true for composite materials failing in fragmentation, brittle fracture, or fiber splaying failure modes.[1-6] The equation for SEA is

$$SEA = \frac{W}{A\rho\delta}. \qquad \text{(A.2)}$$

A.1.2 Specific Sustained Crushing Stress (SSCS)

SSCS is the average stress during stable crushing divided by the density of the material. It has several advantages and disadvantages over the SEA method of measurement.

Advantages

- It is simple: it requires only an average load from the load curve

- It can be used to compare specimens with different crush distances, but only if the load is consistent during stable crush
    - The relative size of the initial portion of the load curve does not effect the results

Disadvantages

- The stable crushing region needs to have a consistent load
    - Increasing, decreasing, or erratic loads do not give accurate average load results
- It cannot measure samples that do not experience stable crush
- The initial point of stable failure must be selected carefully

This initial point of stable crushing can be determined several ways. The initial slope of the curve represents the failure of the trigger (seen in Figure A.1 as the portion of the curve up to 11mm of displacement). There is often a very obvious peak at the end of this slope followed by a sudden drop in load after which stable crushing occurs. Stable crush is said to begin at the first local minimum after the peak load. Therefore, the average load used in the SSCS calculation is the average load from this local minimum to the end of stable crush, which is dependent on the total crushed distance of the tube.

For specimens that do not have an obvious peak a 90% rule can be used. That is, stable crush is said to begin at the point after the peak load of the initial slope where the load is 90% of the peak load (see Figure A.2). The average load is then the average of the load from this point to the end of stable crush.

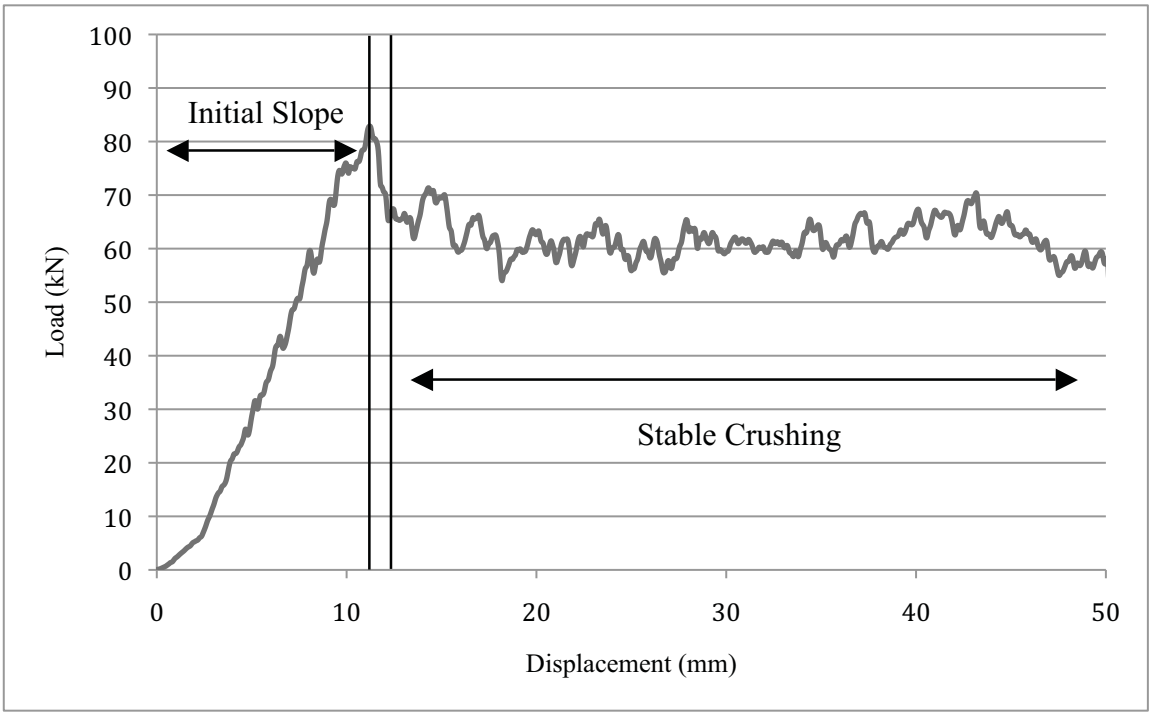

Figure A.1: Sample load curve showing points and regions of interest.

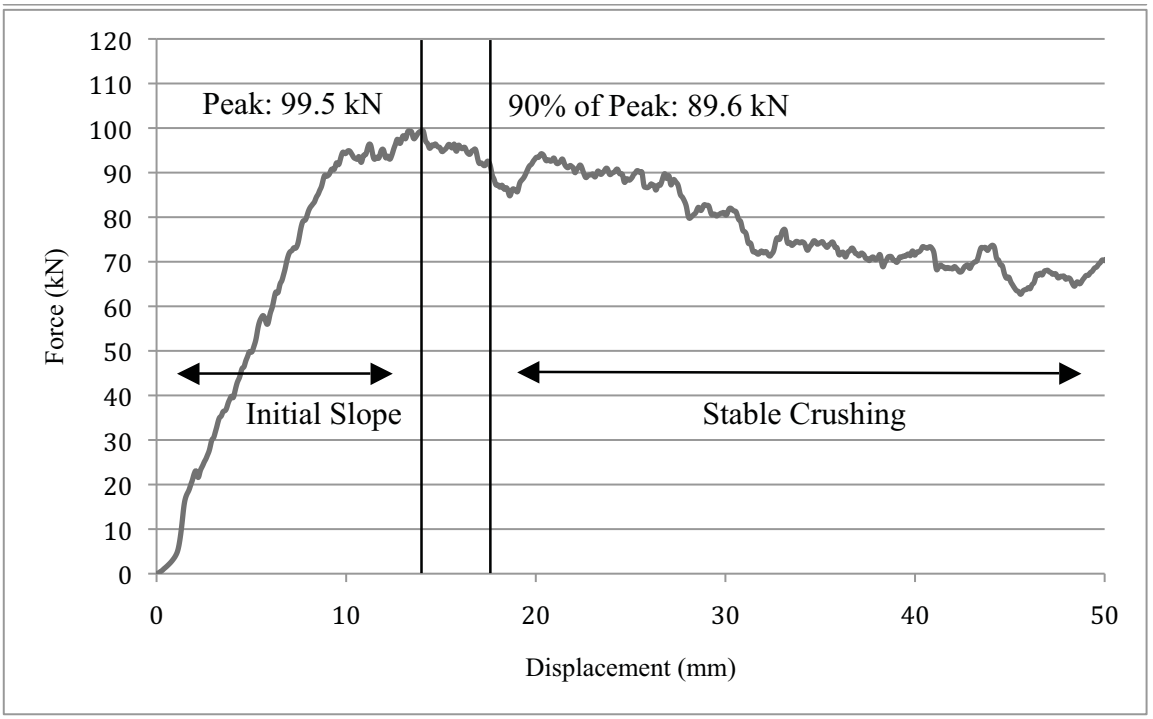

Figure A.2: Sample curve calculations using the 90% rule.

The average load obtained by either of the methods described above is divided by the average specimen area to get average stress (σ) and then divided by average density (ρ) to get SSCS.

$$SSCS = \frac{\overline{\sigma}}{\rho} \tag{A.3}$$

A.2 Mechanical Test Machine Data

Mechanical testing was performed on an Instron 50,000 lbf electromechanical universal test machine. The raw data from testing was stored as load versus displacement data. Displacement values were positive in the up direction (tension), with the zero being the crosshead location at the start of the test. To allow for data analysis of compression tests the displacements were multiplied by -1 to yield positive numbers. To show accurate displacements the offset distance of the crosshead (see Figure A.3) was subtracted from all displacement data. The resulting final curves were similar to that shown in Figure A.1.

A.3 Testing Machine for Automotive Composites (TMAC)

TMAC is an open loop servo-hydraulic test machine capable of constant crushing velocities of up to 8 m/s. It is located at Oak Ridge National Laboratory in Oak Ridge, TN. TMAC has an integrated 500 kN load washer located under the specimen mounting base. A position transducer is located on the hydraulic ram. Raw data from testing were stored as load versus displacement data. The only modification necessary to the data was to offset the displacement to 0 using a procedure similar to that for the mechanical test machine discussed in Section A.2.

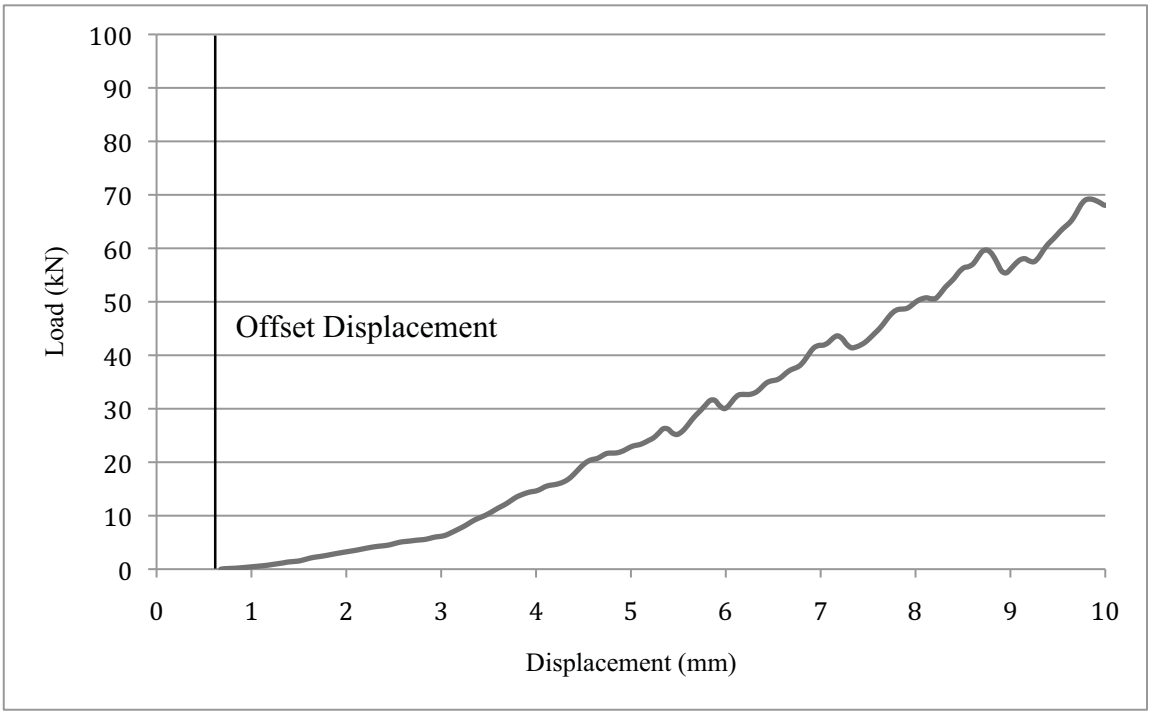

Figure A.3: Load versus displacement curve showing an initial offset.

A.4 Drop Tower Data

A.4.1 Raw Data

Drop tower testing was performed on a 3 m drop tower with a load cell located on the top of the base frame, below the test sample (Figure A.4). The mass of the drop weight was 73.2 kg. Raw data from testing was stored as load versus time data. The time was offset to 0 using the same procedure as that for displacement shown in Section A.1. In order for the data to be consistent with quasi-static testing data it was converted into force versus displacement data using equations of motion. It was assumed that the acceleration of the drop mass was constant between each data point (represented as time 1 (t_1) and time 2 (t_2)). The equations of motion are therefore:

$$F = ma \tag{A.5}$$

$$v_2 = v_1 + a(t_2 - t_1) \tag{A.6}$$

$$x_2 = x_1 + v_1 t + (1/2)a(t_2 - t_1)^2 \tag{A.7}$$

These equations of motion were applied to each time step. The resulting curves were force versus time, acceleration versus time, velocity versus time, and force versus displacement. See Figures A.5-A.8. Each force versus displacement curve was integrated using the trapezoidal method to find the total energy absorbed by each specimen. This value was compared to the theoretical value of kinetic energy for the cross head at the moment before impact to give a check to the accuracy of the data. A sample calculation is shown on Figure A.8 with the theoretical energy and the measured energy found from the load curve using the trapezoidal rule for integration.

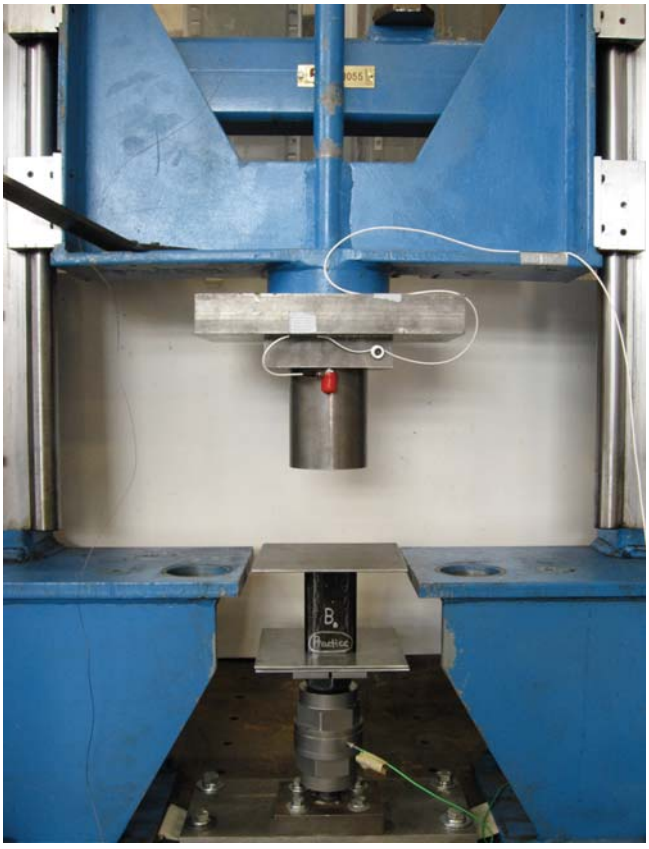

Figure A.4: Drop tower load cell configuration.

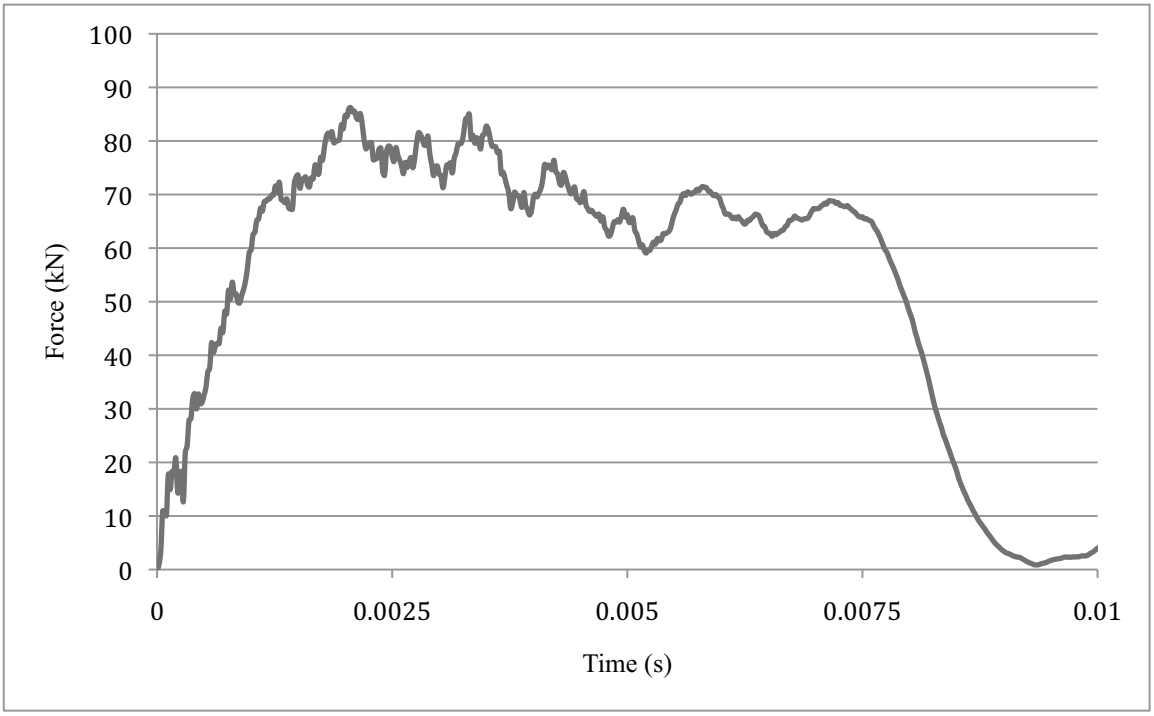

Figure A.5: Drop tower force versus time curve.

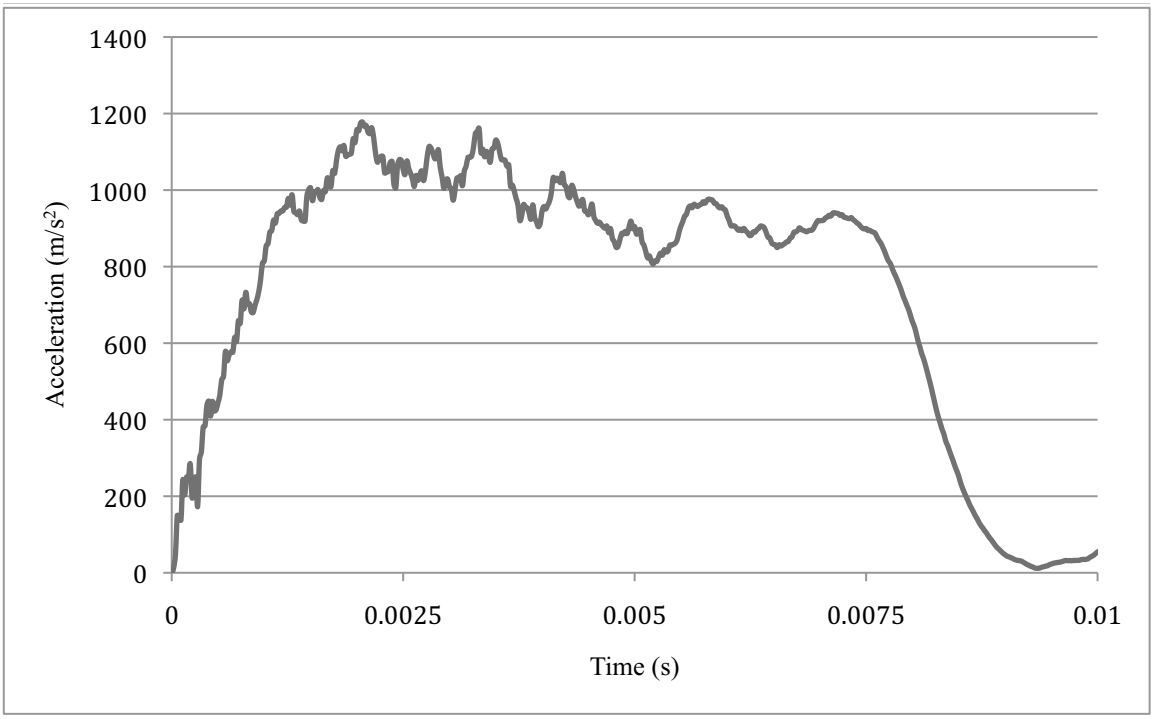

Figure A.6: Drop tower acceleration versus time curve.

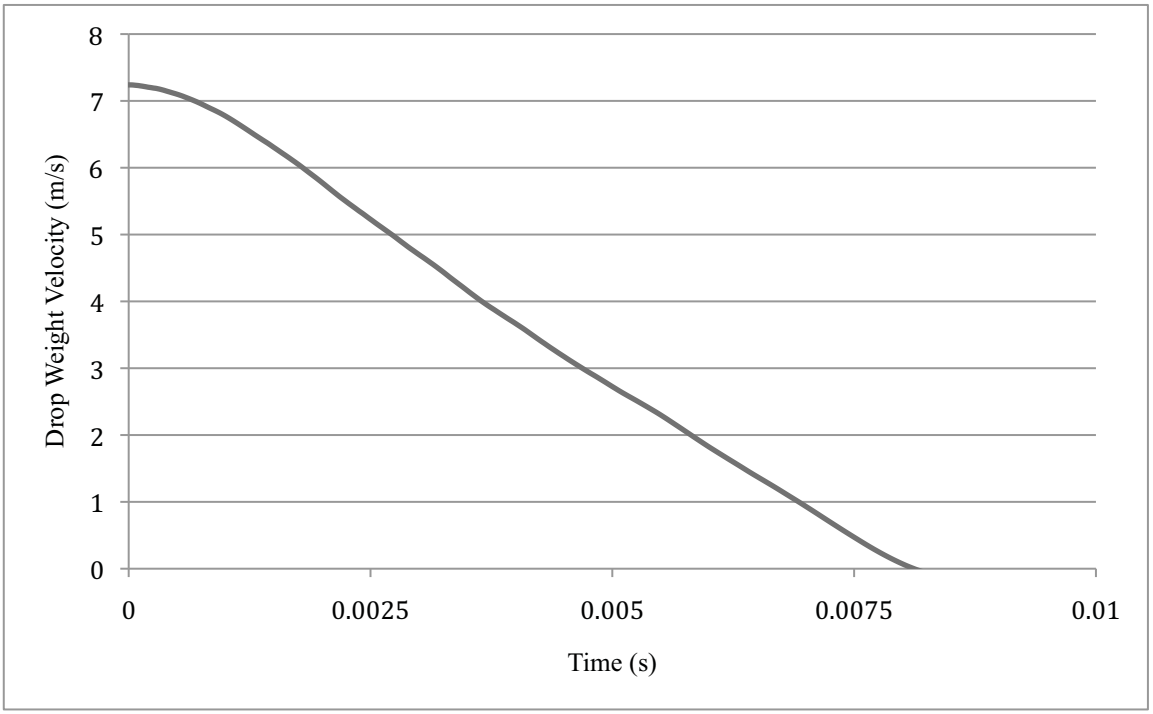

Figure A.7: Drop tower velocity versus time curve.

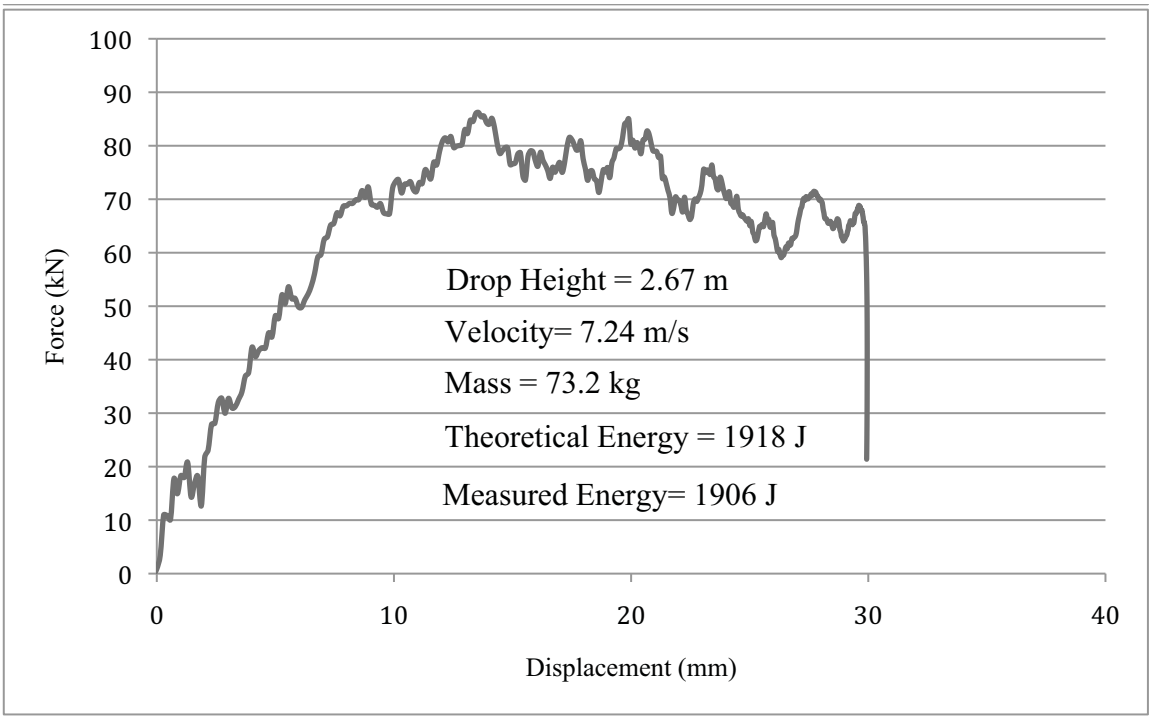

Figure A.8: Drop tower force versus displacement curve.

A.4.2 Evaluating SEA or SSCS

The data from the drop tower were taken at a fixed frequency. As the drop weight slowed during crushing the displacement between recorded data points became smaller. If using the SEA method of energy absorption characterization equations (A.1) and (A.2) could be used directly since the trapezoidal method takes into account the distance between data points. However, if using the SSCS method described in Section A.2.2 additional calculations had to be performed or the average load would be incorrect. A weighted average method was used where the weight (w_n) was the displacement between points (n) and (n+1).

$$p_{mean} = \frac{\sum_{1}^{n} w_n \left(\frac{f(n) + f(n+1)}{2} \right)}{\sum_{1}^{n} w_n} \tag{A.8}$$

An example of the error introduced through a pure average of the load is shown in Figure A.9 for a test sample that experienced a decreasing load during stable crushing.

A.5 Comparison of Data From Different Test Types

It was often necessary to compare data from mechanical, drop tower, and servo hydraulic tests. This was easily done, but several considerations needed to be taken into account.

If using the SEA method it was necessary that the data being compared have the same displacement. The initial slope of the curve has comparatively less energy absorption than the stable crush region of the curve due to the load starting at 0. The effect this lower

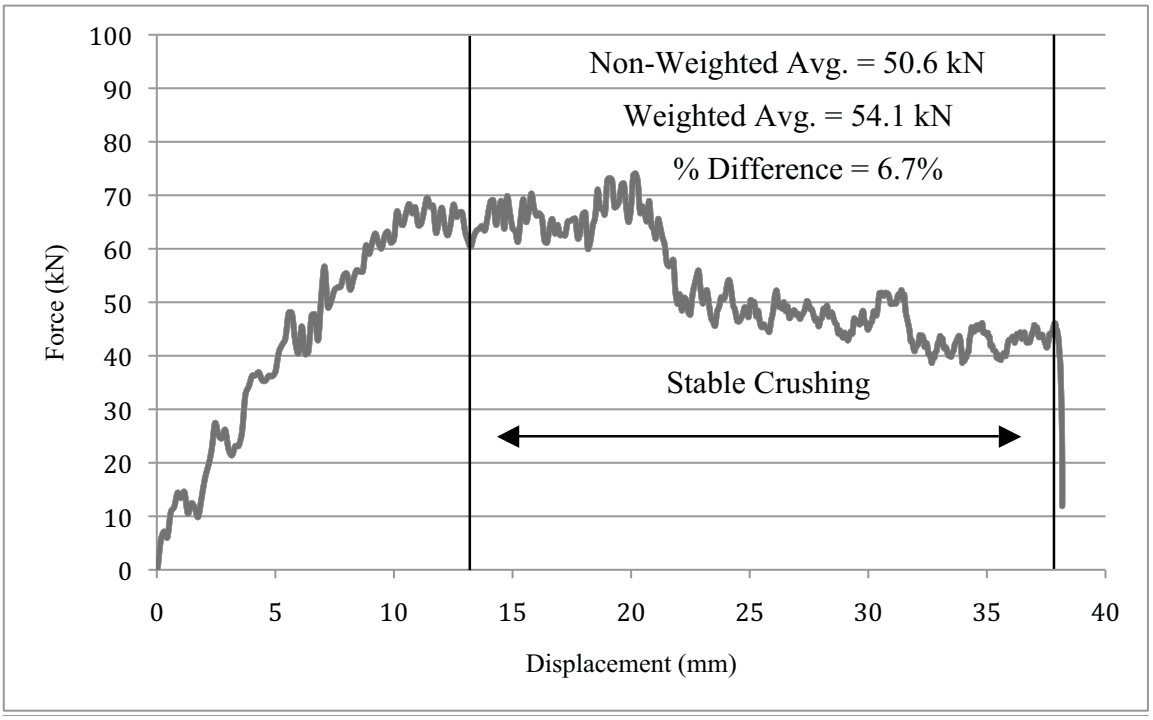

Figure A.9: Drop tower curve and resulting average load and weighted-average load.

energy has on the resulting SEA value is determined by the length of the initial slope and the overall length that the test sample is crushed.

When finding the average load for the SSCS method it was necessary that equal displacement curves were used. Figure A.10 shows test results for the same test sample type tested on a drop tower and mechanical test machine. It is difficult to predict what the drop tower load curve will do from 30 mm to 50 mm of displacement. If comparing these two curves the mechanical test machine data should be truncated to 30 mm.

It should be noted that it is possible for the average force during stable crush to be independent of displacement. For these types of curves the average stress used in the SSCS method would not be dependent on the length of the curve. However, it was observed that this happens rarely and therefore it is advised that the curves are always of the same displacement.

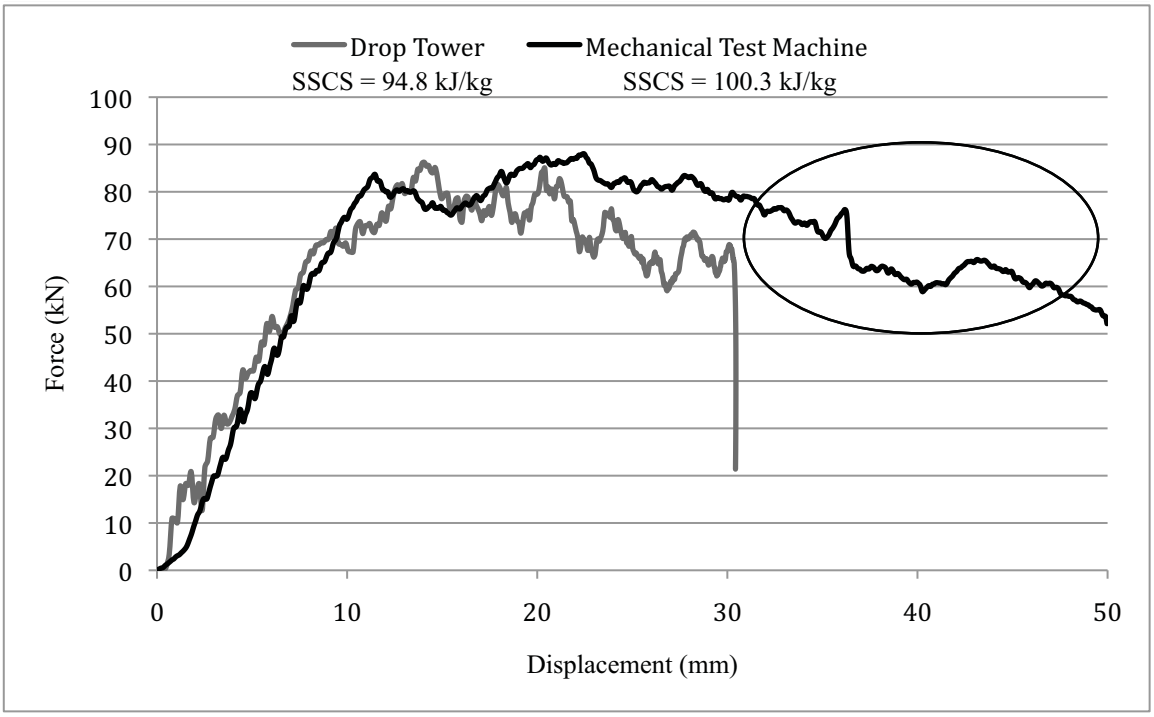

Figure A.10: Resulting quasi-static and drop tower data for similar tube samples.

A.6 References

1. D. Hull, "A Unified Approach to Progressive Crushing of Fiber-Reinforced Composite Tubes," Composite Science and Technology 40 (1991), 377-421.

2. D. Hull, "Energy Absorption of Composite Materials Under Crash Conditions," Progress in Science and Engineering of Composites (1982), T. Hayashi, K. Kawate and S. Umekawa, (eds), 861-870.

3. A.G. Mamalis and D.E. Manolakos, "Crashworthy Behavior of Thin-Walled Tubes of Fibreglass Composite Materials Subjected to Axial Loading," Journal of Composite Materials 24 (1990), 72-91.

4. G.L. Farley, "Effect of Fiber and Matrix Maximum Strain on the Energy Absorption of Composite Materials," Journal of Composite Materials 20 (1985), 322-334.

5. T.J. Brimhall, "Friction Energy Absorption in Fiber Reinforced Composites," Thesis (2005), Michigan State University.

6. G.C. Jacob, "Automotive Crashworthiness of Adhesively Bonded Carbon Fiber Polymer Composite Structures," Thesis (2006), University of Tennessee.

APPENDIX B

FORCE VERSUS DISPLACEMENT CURVES

B.1 Characteristics of Load Curves

During crush testing it was observed that testing variables could affect the characteristics of the force versus displacement curve. For example, tulip triggered tubes were shown to have smaller initial slopes when compared to bevel triggers. This may be desirable in certain situations because it would provide lower initial accelerations during an impact. Other load curve characteristics may also offer advantages in certain situations, therefore, example curves for each of the test groups are provided below.

The load versus displacement curves from tubes test quasi-statically (4.23×10^{-4} m/s) and dynamically (6 m/s) were observed to have similar characteristics, although dynamic curves experienced oscillations due to the ringing of the load cell. This made the true load versus displacement curve for dynamic tests more difficult to visualize. For this reason, quasi-static curves representing each test group are given in Figures B.1-B.12.

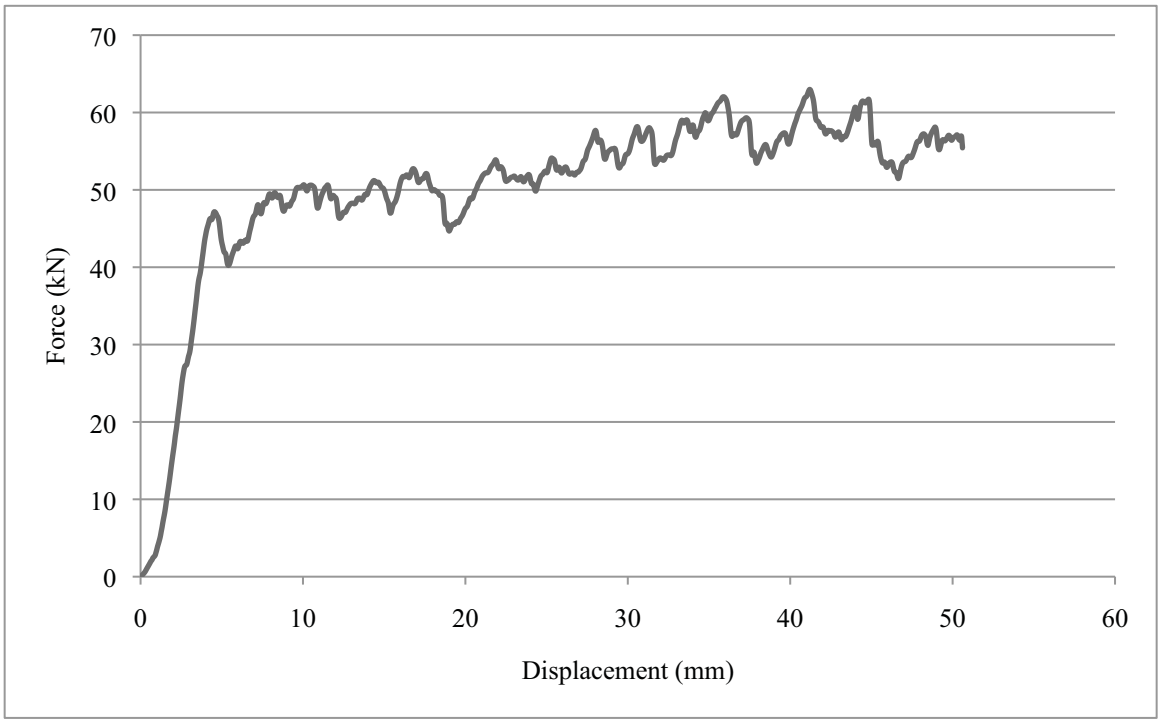

Figure B.1: Circular tube with [F] layup and bevel trigger.

Figure B.2: Circular tube with [F] layup and tulip trigger.

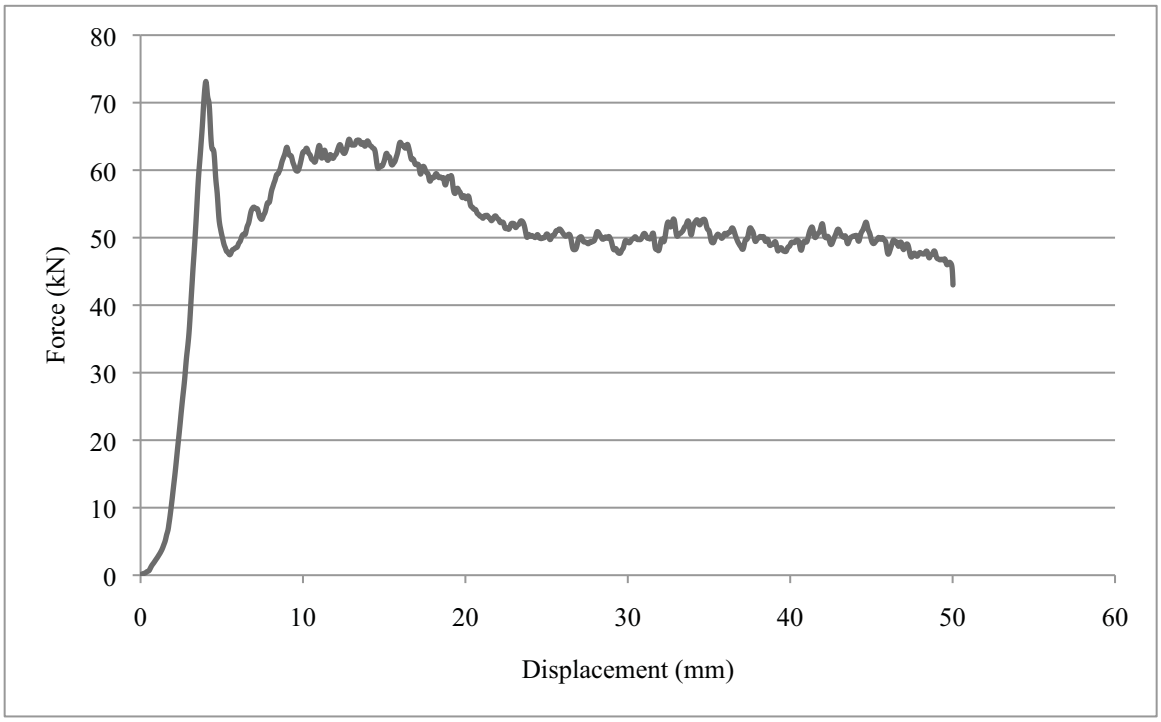

Figure B.3: Circular tube with [B] layup and bevel trigger.

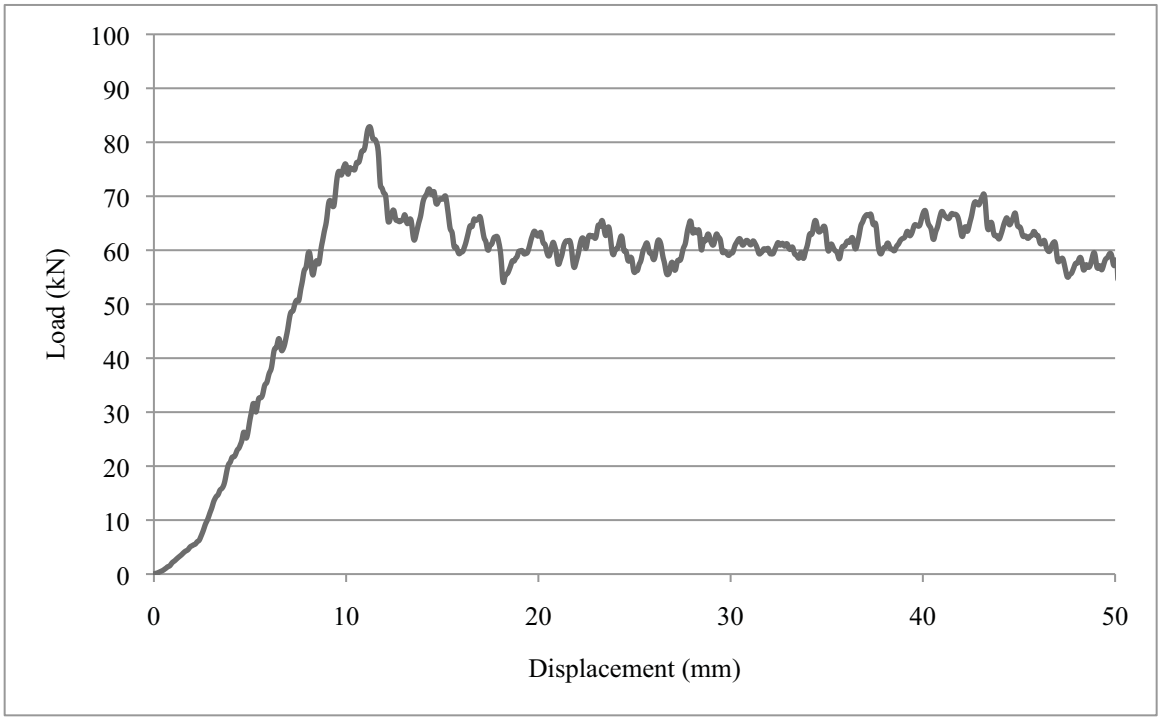

Figure B.4: Circular tube with [B] layup and tulip trigger.

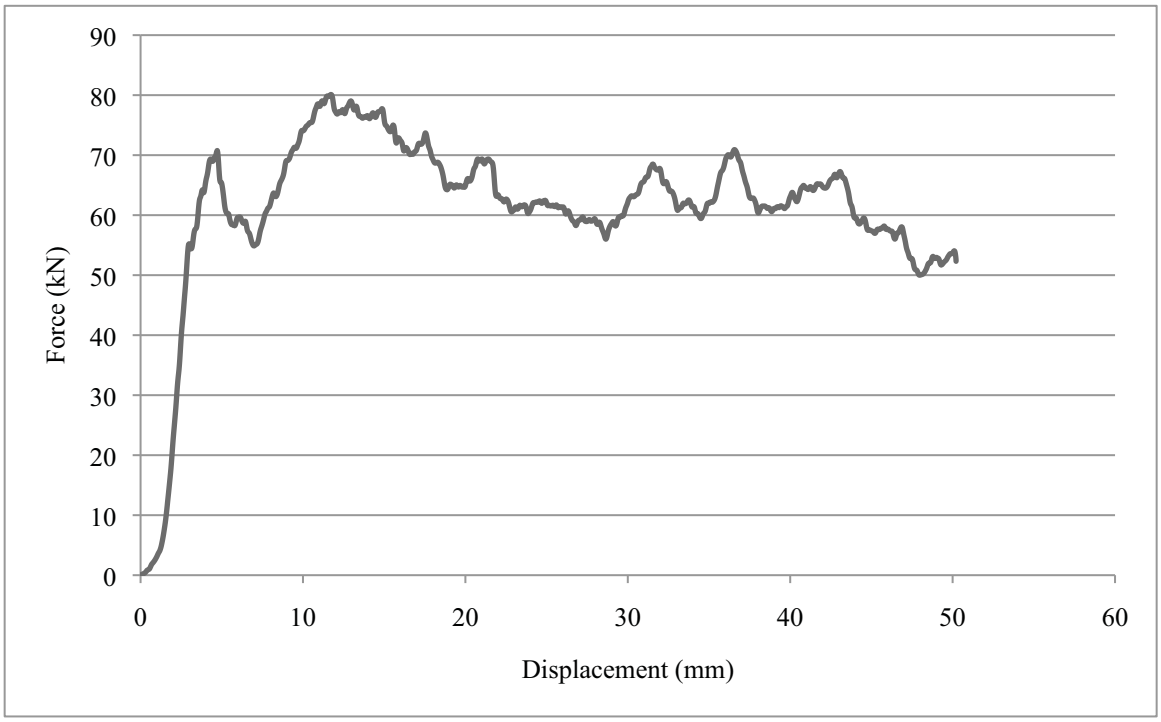

Figure B.5: Circular tube with [S] layup and bevel trigger.

Figure B.6: Circular tube with [S] layup and tulip trigger.

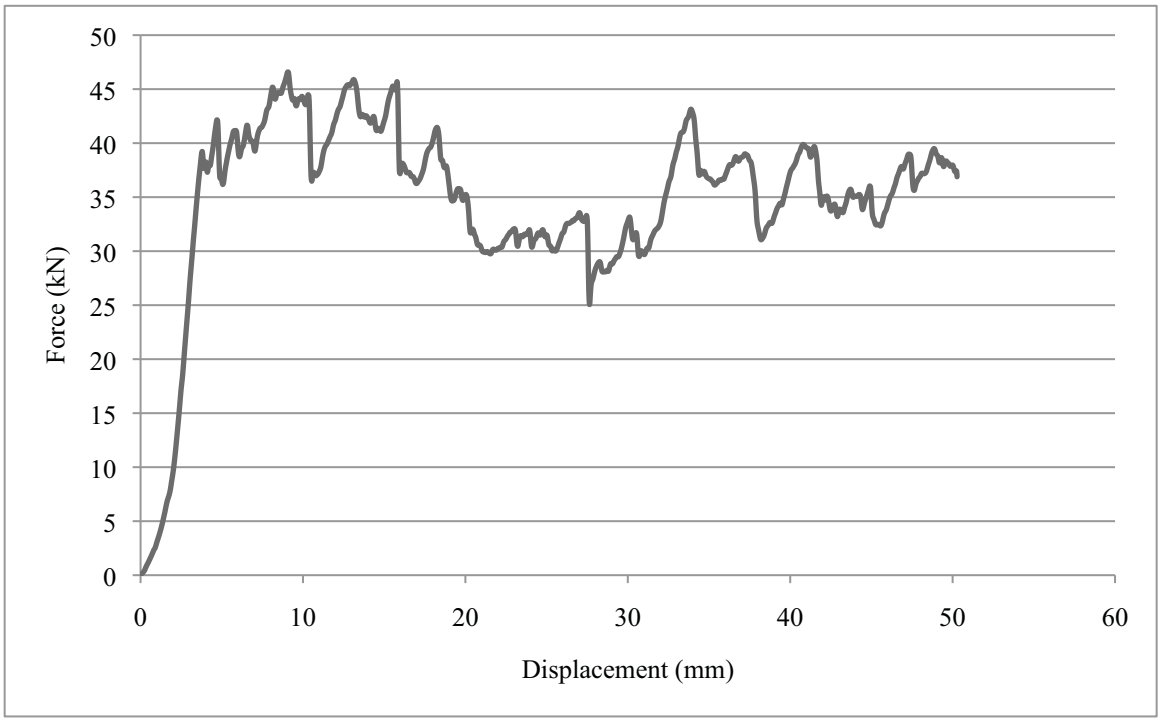

Figure B.7: Square tube with [F] layup and bevel trigger.

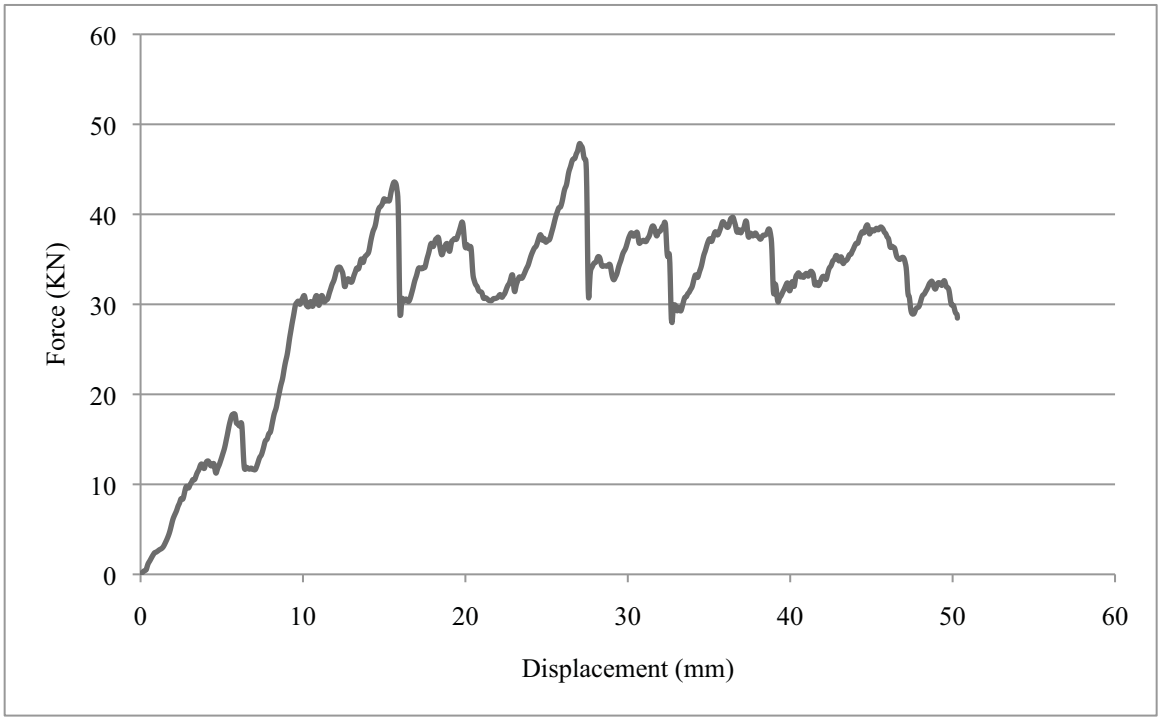

Figure B.8: Square tube with [F] layup and tulip trigger.

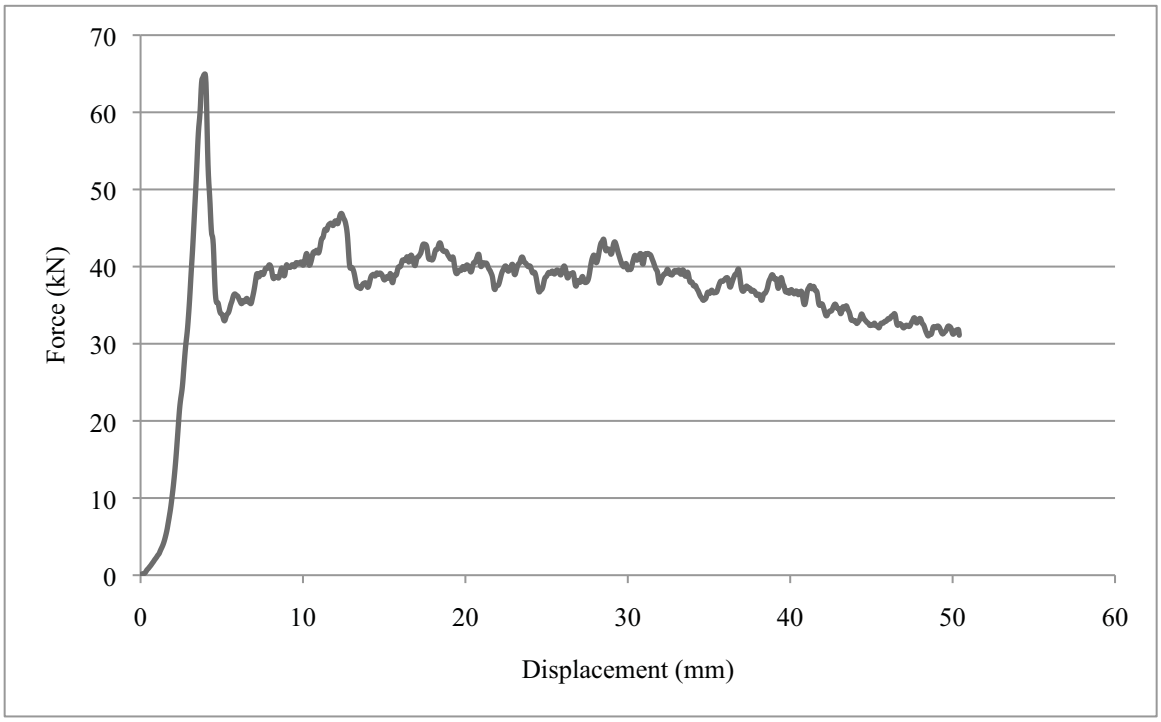

Figure B.9: Square tube with [B] layup and bevel trigger.

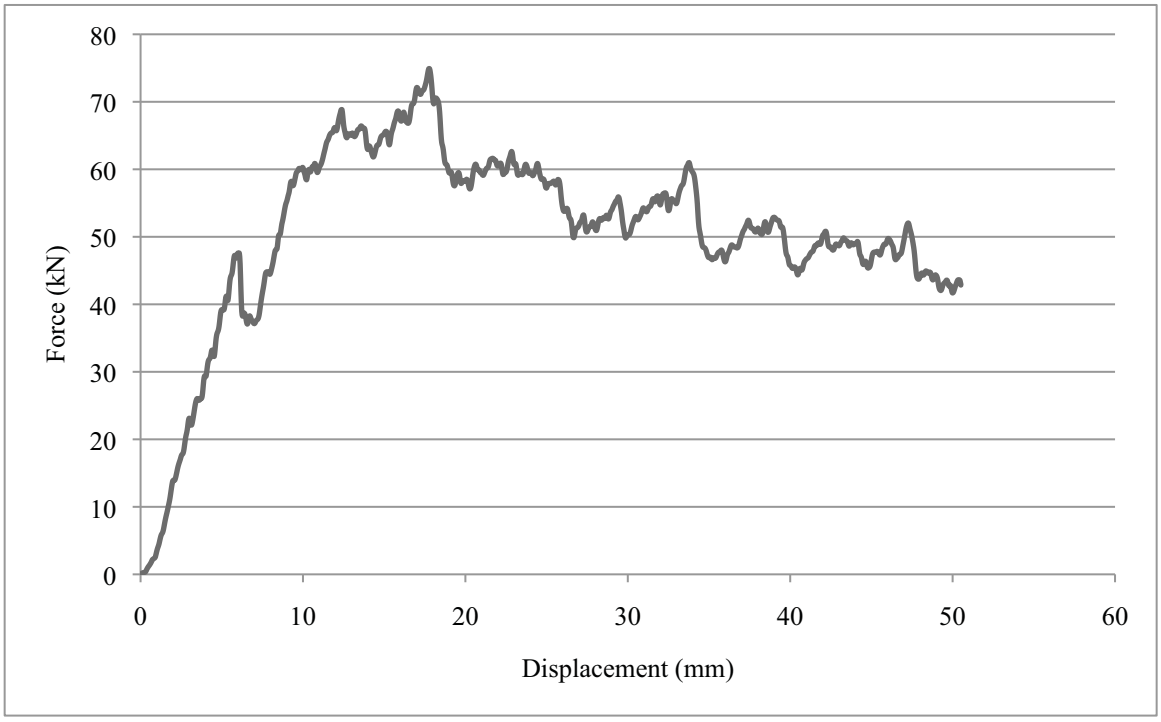

Figure B.10: Square tube with [B] layup and tulip trigger.

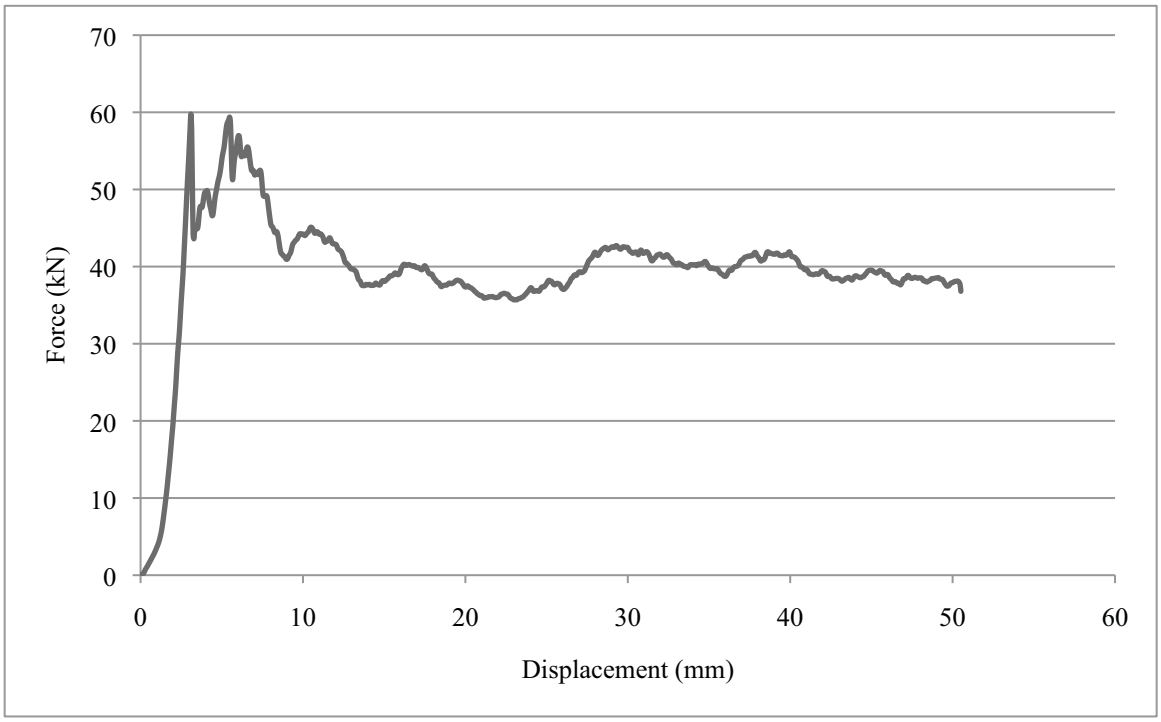

Figure B.11: Square tube with [S] layup and bevel trigger.

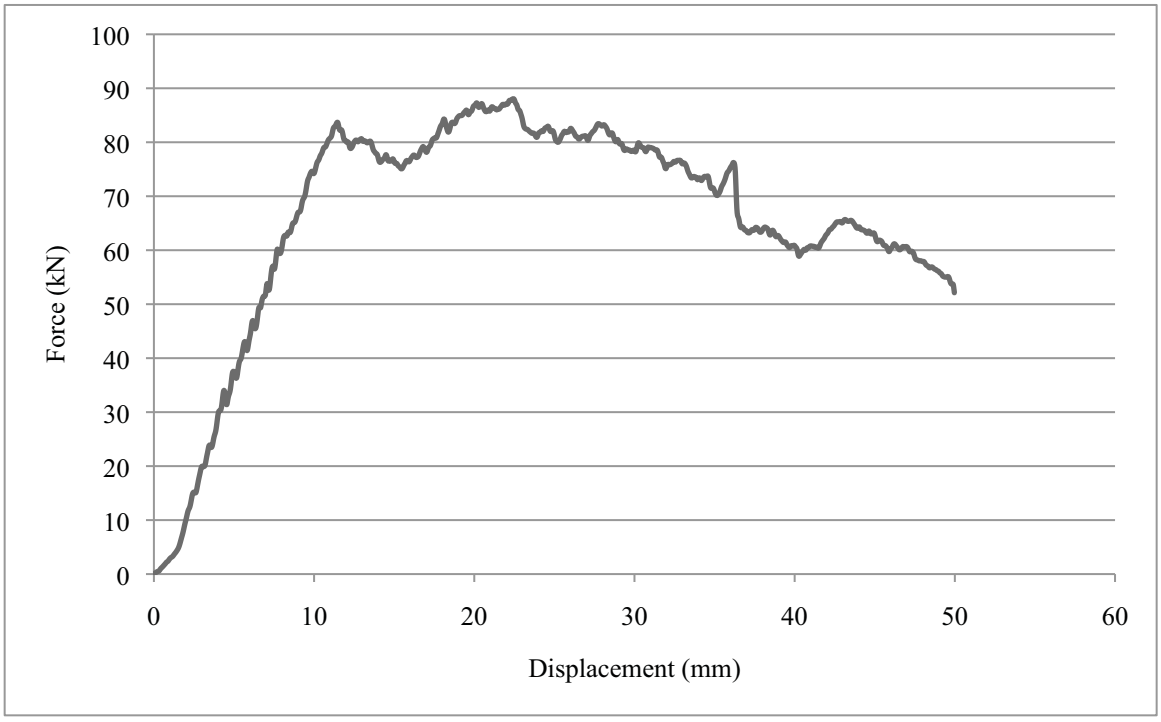

Figure B.12: Square tube with [S] layup and tulip trigger.